remote sensing

MDPI

Article

Effect of Assimilating SMAP Soil Moisture on CO_2 and CH_4 Fluxes through Direct Insertion in a Land Surface Model

Zhen Zhang [1,*], Abhishek Chatterjee [2,3,†], Lesley Ott [2], Rolf Reichle [2], Andrew F. Feldman [4] and Benjamin Poulter [4]

1 Earth System Science Disciplinary Center, University of Maryland, College Park, MD 20740, USA
2 Global Modeling and Assimilation Office, NASA Goddard Space Flight Center, Greenbelt, MD 20771, USA; abhishek.chatterjee@jpl.nasa.gov (A.C.); lesley.e.ott@nasa.gov (L.O.); rolf.reichle@nasa.gov (R.R.)
3 Universities Space Research Association, Columbia, MD 20771, USA
4 Biospheric Sciences Laboratory, NASA Goddard Space Center, Greenbelt, MD 20771, USA; andrew.feldman@nasa.gov (A.F.F.); benjamin.poulter@nasa.gov (B.P.)
* Correspondence: zzhang88@umd.edu
† Current address: NASA Jet Propulsion Laboratory, California Institute of Technology, Pasadena, CA 91326, USA.

Abstract: Soil moisture impacts the biosphere–atmosphere exchange of CO_2 and CH_4 and plays an important role in the terrestrial carbon cycle. A better representation of soil moisture would improve coupled carbon–water dynamics in terrestrial ecosystem models and could potentially improve model estimates of large-scale carbon fluxes and climate feedbacks. Here, we investigate using soil moisture observations from the Soil Moisture Active Passive (SMAP) satellite mission to inform simulated carbon fluxes in the global terrestrial ecosystem model LPJ-wsl. Results suggest that the direct insertion of SMAP reduces the bias in simulated soil moisture at in situ measurement sites by 40%, with a greater improvement at temperate sites. A wavelet analysis between the model and measurements from 26 FLUXNET sites suggests that the assimilated run modestly reduces the bias of simulated carbon fluxes for boreal and subtropical sites at 1–2-month time scales. At regional scales, SMAP soil moisture can improve the estimated responses of CO_2 and CH_4 fluxes to extreme events such as the 2018 European drought and the 2019 rainfall event in the Sudd (Southern Sudan) wetlands. The simulated improvements to land–surface carbon fluxes using the direct insertion of SMAP are shown across a variety of timescales, which suggests the potential of SMAP soil moisture in improving the model representation of carbon–water coupling.

Keywords: data assimilation; land surface model; methane; remote sensing; dynamics global vegetation model

Citation: Zhang, Z.; Chatterjee, A.; Ott, L.; Reichle, R.; Feldman, A.F.; Poulter, B. Effect of Assimilating SMAP Soil Moisture on CO_2 and CH_4 Fluxes through Direct Insertion in a Land Surface Model. *Remote Sens.* **2022**, *14*, 2405. https://doi.org/10.3390/rs14102405

Academic Editor: Gabriel Senay

Received: 17 March 2022
Accepted: 13 May 2022
Published: 17 May 2022

1. Introduction

Soil moisture plays a critical role in controlling interactions between the soil, vegetation, and atmosphere, and is one of the major drivers that affects the carbon fluxes of terrestrial ecosystems [1]. Because of the coupling between water and carbon fluxes at the leaf level, soil moisture is a major constraint for the assimilation of carbon by vegetation through photosynthesis [2]. Soil moisture is the dominant driver of dryness stress on ecosystem production across more than 70% of vegetated land areas [3]. The spatial and temporal variations in soil moisture strongly affect the terrestrial carbon uptake [4]. Meanwhile, soil moisture serves as a proxy for water table depth, a variable that regulates the soil redox state for microbes to favor methanogenesis, which is used to determine the time and location of inundated areas at a regional scale that can significantly affect the estimate of methane (CH_4) flux [5]. Therefore, it is essential to understand the spatio-temporal distribution of soil moisture and its role in influencing terrestrial carbon fluxes in a warming climate.

Understanding the influence of soil moisture on terrestrial carbon fluxes is challenging because of the large uncertainty in the spatio-temporal distributions of soil moisture, which

is due to both its high spatial heterogeneity and uncertainty in characterizing surface properties. A common approach to estimate soil moisture is through land surface model simulations driven with surface meteorological forcing data from observations or atmospheric reanalysis systems. This approach depends on the appropriate parameterization of hydraulic parameters and soil texture [6], model structure, and external forcings from the meteorological datasets. These models can produce vast differences in soil moisture even with the same forcings [7]. Previous studies have explored the impact of soil moisture on past and future CO_2 fluxes using prognostic models [1,4,8–11]. These studies show that the influence of soil moisture on carbon fluxes is still affected by bias and remains unclear, given the various sources of uncertainty that prevail in the models [12–14].

Satellite observations of soil moisture have become increasingly available during the past decade and provide much needed information at the global scale [15–20]. These soil moisture observations are based on radar (active) or radiometer (passive) measurements of low-frequency microwave signals. The European Space Agency's Soil Moisture Ocean Salinity (SMOS; [21]) mission and the NASA Soil Moisture Active Passive (SMAP; [22]) missions were specifically designed for measuring soil moisture, and both carry L-band radiometers (1.41 GHz). Compared to C- and X-band data from sensors such as the Advanced Scatterometer (ASCAT), L-band measurements have the advantage of deeper penetration through vegetation canopies and into the soil, leading to a higher accuracy of the soil moisture signals received [18,23]. A recent comprehensive evaluation of satellite- and model-based soil moisture products suggests that SMAP outperforms other satellite-based datasets when compared to in situ soil moisture measurements [24]. Future satellite missions, such as NASA Surface Water and Ocean Topography (SWOT) and NASA-ISRO SAR (NISAR), will continue to improve the monitoring and understanding of soil moisture.

Assimilating satellite-based observations of soil moisture into terrestrial carbon cycle models provides a potential opportunity to reduce the uncertainty of carbon flux estimates. Data assimilation approaches have previously been applied to integrate soil moisture observations into the models over different climatological and hydrological environments. Past data assimilation studies have primarily focused on improving hydrologic modeling by addressing seasonal dynamics [25–28]. The NASA SMAP Level 4 Carbon product (L4_C Version4, Greenbelt MD, USA) provides estimates of net ecosystem CO_2 exchange (NEE) from a simple terrestrial carbon flux model constrained with the SMAP Level 4 soil moisture data assimilation product [29]. Surprisingly, few studies have investigated the potential of directly assimilating information from satellite soil moisture observations into a terrestrial ecosystem model with full water–carbon coupling at the global scale to constrain the simulated CO_2 fluxes, and we are not aware of any such studies investigating CH_4 fluxes. For example, the author of [30] demonstrates that the assimilation of soil moisture observations from SMOS has a high potential for reducing uncertainty in the gross and net CO_2 fluxes, while [31] uses a direct insertion of a remote sensing-based Leaf Area Index to improve several components of land surface. Recently, Ref. [32] simultaneously optimized model parameters for CO_2 concentration and model state for soil moisture by assimilating SMOS soil moisture observations. These studies show potential to improve the modeling of carbon fluxes in a model–data fusion framework.

The objective of the present paper is to investigate whether modeled CO_2 and CH_4 fluxes can be improved by constraining soil moisture using SMAP observations in the LPJ-wsl terrestrial ecosystem model [33,34]. We present evidence that assimilating SMAP observations into a terrestrial ecosystem model yields significant benefits for the simulated CO_2 and CH_4 fluxes at the global scale. In our feasibility study, we use the Level 3 Global Daily 36 km passive soil moisture retrievals from SMAP (L3SMPE Version 6, Greenbelt MD, USA) to adjust the LPJ-wsl model estimates whenever a SMAP observation is available. We carry out a set of model sensitivity tests to evaluate the impact of assimilating SMAP observations into different representative depths of the model soil moisture. To evaluate the simulated soil moisture and CO_2 fluxes, we use ground observations from the FLUXNET2015 [35] and FLUXNET-CH4 datasets [36]. Wavelet analysis [37,38] is applied

to evaluate the influence of SMAP data assimilation on the performance of modeled CO_2 and CH_4 fluxes for wetland sites in the time–frequency domain. We also select two extreme climatic events, a drought and a flood event, as examples to explore the implications of SMAP data assimilation for carbon cycle research.

2. Materials and Methods

2.1. LPJ-Wsl Terrestrial Ecosystem Model

2.1.1. Hydrology Scheme

The terrestrial ecosystem model LPJ-wsl is a process-based land surface model developed for simulating the fully coupled water and carbon budget of the terrestrial biosphere based on the development of the LPJ dynamic global vegetation model [33]. LPJ-wsl includes land surface processes, such as hydrology [39], the soil biogeochemical cycle, and vegetation dynamics that are represented by plant functional types (PFTs). The distribution of PFTs is simulated based on a set of bioclimatic limits and physiological parameters that govern the establishment of and the competition for resources. Using the modified-LPJ approach of [40] that integrates freeze/thaw cycles in the representation of soil hydrology, the soil column has a depth of 1000 cm, split into the top 200 cm, referred to as soil, and the bottom 800 cm, as the buffer for soil temperature calculation. The upper 200 cm of soil is represented by eight vertically discretized layers with thicknesses of 10, 10, 10, 20, 20, 30, 50, and 50 cm. The lower 800 cm buffer is split into four layers with thicknesses of 82, 135, 221, and 362 cm. The original two-bucket model of LPJ, with an upper layer of 0–50 cm and a lower layer of 50–200 cm, provides soil moisture that corresponds to the top four soil layers (10, 10, 10, and 20 cm) and the bottom four soil layers (20, 30, 50, and 50 cm), respectively, in the updated multiple-soil-layer scheme of LPJ-wsl. The hydrology scheme describes the diffusion of water according to the physical soil properties, which are prescribed using a look-up table of 13 soil types following the distribution of a global texture map from the Harmonized World Soil Database [41], with water-holding capacity estimated using a set of empirical equations [6]. The hydrology module also includes a dynamic snow module and a freeze/thaw module, which allow the model to simulate the permafrost processes [34]. The soil moisture at different vertical levels is computed at a daily time step as influenced by rain infiltration, percolation, evaporation, transpiration, and surface and sub-surface drainage.

Within the upper 0–50 cm of the soil, the daily change in water content Δw_i (mm) in each layer i is calculated as:

$$\Delta w_i = \frac{\left(P + M - E_s - T_{up} - R_{perc}\right)\Delta z_i}{\Delta z_{up}},\ i \leq 4 \quad (1)$$

where P is precipitation, M is meltwater from the snow layer, E_s is bare soil evaporation, T_{up} is transpiration from the upper soil layer, i.e., transpiration weighted by the root fraction in the upper 0–50 cm soil layer, R_{perc} is percolation to the lower 50–200 cm soil layer, Δz_i is the depth of soil layer i, and Δz_{up} is the depth of the upper soil layer (50 cm). The water allocation is proportional to the depth of the soil layer. When the water content of any soil layer in the upper 0–50 cm of the soil exceeds the actual water holding capacity (i.e., water holding capacity after deducing ice content), the surplus water is added to the surface runoff (R_{surf}). The percolation to the lower (50–200 cm) portion of the soil is allowed when there are water inputs from precipitation and meltwater. The percolation (R_{perc}) is calculated as a function of soil texture (represented as empirical parameter k_1 and k_2) and layer thickness, and declines exponentially with soil moisture:

$$R_{perc} = \frac{\Delta z_i}{\Delta z_{up}} k_1 {w_{up}}^{k_2} \quad (2)$$

where k is soil-type-dependent hydraulic conductivity and w_{up} is the water content of the upper soil layer. The change in water content Δw_i in each of the bottom 4 layers is given by:

$$\Delta w_i = \left(R_{perc} - T_{low}\right) \frac{\Delta zi}{\Delta z_{low}},\ i > 4 \quad (3)$$

where T_{low} is transpiration from the 50–200 cm layer and Δz_{low} is the depth of the lower soil layers (150 cm). If the water content of any lower soil layers exceeds the actual water holding capacity, the water is added to subsurface runoff.

The hydrologic processes affect the soil heat capacity and its thermal conductivity, which are related to the volumetric fractions of the soil physical components, such as the water and ice fractions, as well as whether the soil is mineral or peat. The representation of Hortonian runoff in the LPJ-wsl model considers the effects of a reduction in water infiltration capacity in frozen soils [34]. In general, the model includes the effect of soil moisture on the soil thermal regime and the feedback mechanisms of the soil thermal regime on the water cycle, which means that altering the status of soil moisture can affect the carbon cycle processes directly (through water availability constraints) and indirectly (through the modulation of soil temperature constraints by soil moisture).

2.1.2. LPJ-Wsl Carbon Processes

The net ecosystem exchange (defined positive for a net CO_2 source) in LPJ-wsl is calculated as the balance between carbon uptake from photosynthesis and the losses from ecosystem respiration and fire, excluding carbon fluxes from land use change.

The CH_4 flux calculation is based on a prognostic wetland model as presented in [42], which is a function of the two scaling factors for boreal (F_B) and tropical (F_T) wetlands, soil temperature in the upper 0–50 cm soil layer, the soil moisture-dependent fraction of heterotrophic respiration, and inundation extent as:

$$E(t,x) = A(t,x)\ Rh(t,x)\ (\sigma(x)F_T + (1 - \sigma(x))F_B) \quad (4)$$

where *A(t,x)* and *Rh(t,x)* represent wetland extent (Unit: fraction) and ecosystem respiration (Unit: g C m^{-2} mon^{-1}) of grid cell x at time t, respectively. The Q10 factor $\sigma(x)$ describes the temperature dependence of the ratio of C respired as CH_4 and is calculated as $\exp(T(x) - T_{max})/10$, where T(x) is the soil temperature (Unit: K), T_{max} is 303.35 K, and F_T (0.084) and F_B (0.016) are the tropical and boreal scaling factors, respectively, derived from fitting to match to the estimates from regional inventories for the Hudson Bay lowlands [43] and the Amazon Basin lowland [44].

Inundation is simulated by a TOPMODEL hydrological framework [34], which determines the area fraction with soil water saturation from the knowledge of the mean watershed water table depth and a probability density function of combined topographic and soil properties. LPJ-wsl has been applied in carbon cycle studies [45] and has been evaluated using global inventory data sets and satellite observations. The simulated dynamics of wetland area and CH_4 emissions have been evaluated against large-scale observations in previous studies [34,46–48].

2.2. SMAP Soil Moisture

Since 31 March 2015, SMAP has been continuously observing L-band surface brightness temperature emission from the Earth with near-global revisit coverage every 2–3 days, repeating the same ground track every eight days, and with a spatial resolution of ~40 km^2. Here, we use Version 6 of the SMAP Level 3 daily soil moisture retrievals on the 36 km EASE grid [49]. The SMAP soil moisture retrieval algorithm derives moisture conditions in the top 5 cm of the soil from the surface brightness temperature observations after correcting for the effects of vegetations and soil surface roughness and using the Mironov dielectric soil mixing model [50,51]. Soil moisture retrievals for times and locations with vegetation canopy water content in excess of 5 kg m^{-2} are considered unreliable. Soil mois-

ture retrievals with quality flags indicating dense vegetation, snow, or freezing temperature were not used here. We used bilinear interpolation to re-project the daily SMAP data from the 36 km EASE grid to the 0.5-degree global grid of our LPJ-wsl simulation.

Traditionally, it is suggested that the microwave satellite soil moisture has varying penetrating depth depending on the soil moisture conditions, with less effective depth on frozen and saturated soils [52,53]. However, some studies suggest that the skin emission depth of L-band microwaves increase with dryness to 1 m in some cases, with 5 cm potentially being a lower bound under wet conditions [54]. Furthermore, since soil moisture is a storage variable with land surface memory [55], soil moisture variations at different soil layers have similar information content. Namely, in wetter ecosystems, SMAP soil moisture in the top 5 cm has similar information content to soil layers much lower (often to 50 cm) [56]. Consequently, SMAP soil moisture suggests the potentials to represent soil storage layer thicknesses of deeper than 5 cm [57]. Therefore, we expect SMAP's utility to extend beyond 5 cm based on these recent findings. Hereafter, we remain with the null hypothesis in the analysis that it represents 5 cm depths, but test alternative hypotheses of SMAP's representation of deeper soil layers.

2.3. Simulation Setups

There are several challenges in directly comparing satellite soil moisture observations and model estimates of soil moisture [7,58,59]. These are largely due to differences in the parameterizations of soil texture information, the difficulty in matching representative soil depths and spatio-temporal resolutions, and the large within-pixel variability in soil moisture. Here, LPJ-wsl soil moisture estimates from the 0–10 cm top layer are the closest model equivalent to the typical sensing depth of 5 cm associated with SMAP retrievals. Thus, we assume that the water content is evenly distributed within the 0–10 cm soil profile in LPJ-wsl and represents the 0–5 cm soil layer. In addition, SMAP measures soil moisture at the specific local overpass time [16], whereas LPJ-wsl simulates daily average soil moisture.

Given these systematic observing and modeling differences between SMAP and LPJ-wsl, we first compare the LPJ-wsl and SMAP soil moisture information via the development of a normalized Soil Wetness Index (*SWI*) [60]:

$$SWI_{i,t} = \frac{x_{i,t} - \overline{minx_i}}{\overline{maxx_i} - \overline{minx_i}} \tag{5}$$

where $x_{i,t}$ represents soil moisture at grid cell i at time t, and $\overline{minx_i}$ and $\overline{maxx_i}$ represent the mean annual minimum and maximum of soil moisture at grid cell i, respectively. We determined $\overline{minx_i}$ and $\overline{maxx_i}$ for SMAP using April 2015–December 2019 observations and for LPJ-wsl using results from the 'baseline' simulation for the same period when SMAP observations are available. In the LPJ-wsl 'assimilation' run, the simulated LPJ volumetric soil moisture at corresponding depth is replaced with soil moisture ${x^+}_{i,t}$ calculated from SMAP SWI at the end of a daily step

$${x^+}_{i,t} = (maxx_i^{LPJ} - minx_i^{LPJ}) \times {SWI_{i,t}}^{SMAP} + minx_i^{LPJ} \tag{6}$$

whenever a SMAP observation is available, such that the SWI for the updated LPJ-wsl soil moisture matches the SWI of the SMAP observation. Note that the SWI-based rescaling does not preserve the mean soil moisture, unlike the cumulative distribution function matching or standard normal deviate rescaling that is widely used in soil moisture data assimilation [26]. That is, soil moisture assimilation using SWI-based rescaling may result in a non-negligible difference in the distribution of soil moisture between the baseline and assimilation runs.

As discussed in Section 2.2, SMAP L3 surface soil moisture may also contain information about soil moisture in deeper layers [61]. We designed experiments to test the sensitivity of assimilating SMAP soil moisture at different depths. Specifically, we conducted two sets of model simulations: (1) a 'baseline' LPJ-wsl simulation without SMAP

assimilation and (2) three "assimilation" schemes that assimilate SMAP soil moisture into LPJ-wsl for different soil depths in the model: 0–10 cm (topsoil layer, denoted LPJ_10), 0–50 cm (top four soil layers, denoted LPJ_50), and 0–200 cm (all 8 soil layers, denoted LPJ_200). The soil moisture values for these soil depths (0–10 cm, 0–50 cm, and 0–200 cm, respectively) were replaced with volumetric soil moisture derived from SMAP SWI using Equation (5). The performance of the different assimilation schemes was tested against in situ measurements to find the best representative depth.

We used surface meteorological forcing data from the Climate Research Unit (CRU v4.05) [62] to run the LPJ-wsl model in this study. CRU forcing data is a global-scale, in situ-based, monthly spatial-interpolated climate dataset for 1901–2019. A weather generator in LPJ is used to generate daily precipitation events based on a wet-day frequency input and a set of linear interpolations with monthly temperature and cloud cover as inputs to calculate daily temperature, photosynthetically active radiation flux, and potential evapotranspiration. The LPJ-wsl simulations include a spin-up phase, which equilibrates the prognostic variables, including vegetation state, soil carbon pools, and soil moisture content. The spin-up run is a 1000-year simulation that recycles the CRU forcing data from 1901–1930 for the spin-up period until the onset of transient simulation in 1901. During the spin-up run, the atmospheric CO_2 concentration is held constant at the pre-industrial level (286.00 ppm). For the transient simulation, the simulation is forced with varying annual atmospheric CO_2 concentrations using data from observations. For the baseline and assimilation runs, the model setup is the same until 31 March 2015 when SMAP is available.

We first compare our baseline to the assimilated version to assess the effect of different assimilating soil depth on simulated soil moisture values. Because the FLUXNET observations are not available for the study period of 2015–2019, we evaluated the simulated average seasonal cycle from the SMAP assimilation period against the observations. The different schemes were compared at regional scales to discuss the effect of the soil moisture assimilation on large-scale carbon fluxes.

2.4. Evaluation Strategy and Statistical Analysis

2.4.1. Benchmark Datasets

Site-level observations of soil moisture and carbon (i.e., CO_2 and CH_4) fluxes from FLUXNET2015 and FLUXNET-CH4 (hereafter, FLUXNET) were used to evaluate the temporal patterns of simulated results. Given that there are systematic differences between the remotely sensed and ground data due to the spatial representativeness, different measurement depths [63], and uncertainty in the LPJ parameterizations, we evaluated soil moisture on the basis of SWI. We used the same minimum and maximum soil moisture values derived from the baseline run for the SWI calculation of the assimilated runs. The FLUXNET soil moisture used in this study are measurements for the top soil layer (0–15 cm) listed in Tables 1 and A1 [35,36,64].

Table 1. List of sites used in the soil moisture and carbon flux assessment.

Site ID	Site Name	Longitude	Latitude	IGBP Biome Type	Duration
US-Prr	Poker Flat Research Range Black Spruce Forest	−147.48	65.12	Evergreen Needleleaf Forests	2010–2014
CA-TP1	Ontario—Turkey Point 2002 Plantation White Pine	−80.55	42.66	Evergreen Needleleaf Forests	2002–2014
US-ARM	ARM Southern Great Plains site- Lamont	−97.49	36.61	Croplands	2003–2012
US-MMS	Morgan Monroe State Forest	−86.41	39.22	Deciduous Broadleaf Forests	1999–2014
US-Oho	Oak Openings	−83.84	41.55	Deciduous Broadleaf Forests	2004–2013
US-Ton	Tonzi Ranch	−120.97	38.43	Woody Savannas	2001–2014
US-Whs	Walnut Gulch Lucky Hills Shrub	−110.05	31.74	Open Shrublands	2007–2014

Regional-level evaluations were also carried out by comparing with one independent satellite soil moisture product and two gridded carbon flux products that were developed based on upscaling eddy covariance measurements. We use the European Space Agency's Climate Change Initiative for Soil Moisture (ESA CCI SM) product, which harmonizes and merges soil moisture retrievals from multiple satellites into a single product at a 0.25° regular grid [65]. The version applied in this study was the v4.07 combined product from 1 January 2015–31 December 2019 at daily time step. The CO_2 flux estimates were based on a net ecosystem exchange estimate from upscaled FLUXNET observations [66,67].

Figure 1 provides a map of the sites for the evaluation of soil moisture and carbon fluxes. The site selection for soil moisture evaluation followed the criteria to represent land cover spanning from evergreen needleleaf forest (ENF) to grasslands, including croplands; all sites were situated within North America. Therefore, we used 7 sites from FLUXNET for comparison with the LPJ-wsl simulated soil moisture and CO_2 fluxes. Because the upland sites do not have measurements of CH_4 fluxes, we used 26 wetland sites from FLUXNET-CH4 (Table A1; [36,64]) to assess the influence of assimilation on CO_2 and CH_4 fluxes at different time scales for different biome sub-types across the globe.

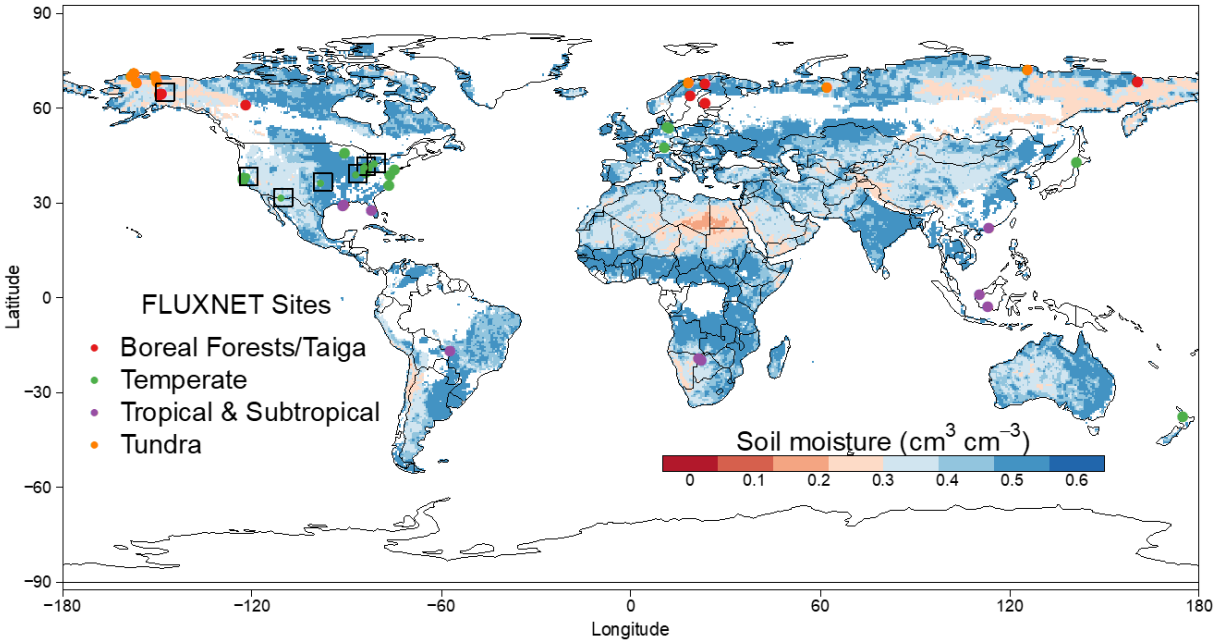

Figure 1. Mean annual maximum of SMAP soil moisture for 2015–2019. Symbols show site locations used in the evaluation, with dots surrounded by rectangles representing the upland sites that are used for the comparison of soil moisture and CO_2 fluxes. The wetland sites used in the evaluation of CO_2 and CH_4 fluxes are grouped into four broad categories according to the classifications from Delwiche et al. (2021). White areas have insufficient good-quality SMAP soil moisture retrievals.

2.4.2. Statistical Analysis and Wavelets

A variety of metrics are applied in this study for evaluating the model performance, which include:

- Root mean standard difference (RMSD) between two datasets;
- Three components of RMSD: squared bias, difference in the magnitude of fluctuation between simulation and measurements $(\Delta\sigma)^2$, and lack of correlation weighted by the standard deviations (LCS), which are used to evaluate the relative skill in reproducing the observations (see below for details);
- The Pearson product–moment correlation coefficient r to assess the relative agreement of the temporal structures between two datasets. The spatial correlation is

also calculated using the same formula but on a single vector of locations at specific time steps;

- Taylor diagrams [68] are used to visually evaluate the relative skill among model-data fits by illustrating the linear correlation coefficient, RMSD, and standard deviation in a polar coordinate plot.

The square of RMSD can be decomposed into three informative components related to bias, the difference in standard deviation between the model and the observations, and the lack of correlation. Specifically, the RMSD can be written as follows [51,60]:

$$RMSD^2 = Bias^2 + VAR + LCS \tag{7}$$

where *bias* is the mean difference between the time series of the model ($x_{i\,=\,1..n}$) and the observations ($y_{i\,=\,1..n}$) for a given location i:

$$Bias^2 = (\overline{x_i} - \overline{y_i})^2 \tag{8}$$

and the square differences of the standard deviations of the model and observations (*VAR*) are expressed as:

$$VAR = (\sigma_{xi} - \sigma_{yi})^2 \tag{9}$$

A large value of VAR indicates that the model fails to simulate the variability. Finally, LCS reflects the lack of correlation (r) between the observations and the model, weighted by the product of the standard deviations:

$$LCS = 2\sigma_{xi}\sigma_{yi}(1 - r) \tag{10}$$

To assess the model behavior of simulating soil moisture and carbon fluxes across space and time, we apply wavelet analysis, a model–data evaluation approach in the frequency domain that has been applied to quantify the variability of CO_2 and CH_4 fluxes across timescales [69–71]. To determine whether/how assimilating SMAP observations every 3–5 days improves the modeled variability at different time scales, we applied wavelet analysis to decompose the (normalized) data–model differences, which is useful to provide insights about data–model disagreements at different temporal scales. Since the modeled carbon fluxes are not directly comparable to the eddy covariance measurements owing to the spatial mismatch between modeled gridded fluxes and site-level observations, we evaluated the simulated CO_2 and CH_4 fluxes by calculating the normalized residual error (NRE) in between LPJ and the observed soil moisture as:

$$\varepsilon_{s,m,t} = \left(\frac{Model_{s,m,t} - \overline{Model_{s,m,t}}}{\sigma_{s,m}}\right) - \left(\frac{Data_{s,t} - \overline{Data_{s,t}}}{\sigma_s}\right) \tag{11}$$

where the subscripts denote site (s), model (m), and time (t), and the overbar denotes the average over the full length of the time series. For each LPJ-wsl simulation experiment, we calculate the spectral characteristics of NRE and compare the spectra to the appropriate null model (i.e., baseline), which is defined as a spectra account for the errors in the flux observations (see Appendix A.1 for more details about the calculation).

3. Results

In Sections 3.1 and 3.2, we first show evidence that assimilating SMAP soil moisture into LPJ improves LPJ's soil moisture representation. This ultimately leads to an improved LPJ representation of carbon fluxes, as shown in Section 3.3, especially in locations where LPJ's baseline soil moisture representation is not reflective of that observed.

3.1. An Analysis of Model Depth Selection

The comparison of site-level soil moisture for different assimilation schemes suggests that the majority of the assimilation experiments showed improved simulations over the baseline in comparison to the FLUXNET measurements, with the degree of improvement depending on the underlying agreement of SMAP with FLUXNET data. The model generally compares closest to FLUXENT when assimilating the SMAP soil moisture for the soil columns 0–50 cm and 0–200 cm, as indicated in Figure 2. The performance of the modeled results also largely depended on the agreement between SMAP and the observation at the evaluation sites. For the boreal site (US-Prr), which showed higher discrepancies between SMAP and FLUXNET, the assimilation runs tended to have little/no improvement against the in situ observations. The spread in performance within biome types was broad: two of the seven sites with the best performance were open shrubland and savanna, where the relatively low vegetation density and low soil organic carbon tended to have less influence on the accuracy of the SMAP soil moisture.

Figure 3 more comprehensively shows the discrepancies between the assimilation schemes' soil moisture values (represented as SWI) and those of the in situ FLUXNET soil moisture values using the decomposed RMSD2 metrics in SWI. It ultimately confirms that several components of LPJ_200 soil moisture compare closely to those of the in situ measurements. In each LPJ-wsl simulation, the bias and LCS with FLUXNET site were considerably reduced after assimilating the SWI from the SMAP soil moisture, while the Var $(\Delta\sigma)^2$ was only slightly affected by the assimilation. This was mainly due to the assimilation of normalized observations, which preserves the variability but alters the seasonality of soil moisture. This indicates that, after the assimilation of SMAP soil moisture, the biases with site-level observations were removed, and the agreement was considerably improved. However, the ability to improve the performance in simulating the variability at the level of individual sites was limited. Since assimilating SMAP into the whole soil column (0–200 cm) in LPJ-wsl had a better performance than the other schemes, we use the LPJ_200 scheme for the remainder of this paper to interpret the effect of soil moisture assimilation on carbon fluxes.

3.2. Site-Level Comparison of Soil Moisture

The comparison of the simulated daily soil moisture with the FLUXNET in situ and SMAP satellite measurements suggested that, by construction, the assimilated results had a better agreement with the SMAP observations. The agreement of the density distribution of SMAP assimilated soil moisture vs. that of FLUXNET strongly depended on the accuracy of the SMAP retrievals in detecting surface soil moisture (Figure 4). At the US-Prr site, the assimilation estimates agreed less well with the in situ measurements than they did with the baseline estimates, owing to the mismatch between SMAP and the in situ data. This was mainly attributed to the effect of the soil freeze/thaw processes on the SMAP retrievals at high latitudes, as suggested by previous studies [72–74], which causes relatively poor performance in the validation. Other than US-Prr, for five of the seven sites (CA-TP1, US-MMS, US-Oho, US-Ton, US-Whs), the assimilated results had better agreement than the LPJ-wsl baseline simulation with FLUXNET in terms of the median value and distribution. For open shrubland and savanna sites (US-Whs and US-Ton), all simulations were comparable with each other, given the reduced influence of vegetation canopies on the SMAP retrievals and the relatively good performance of the LPJ-wsl baseline in dry and temperate regions.

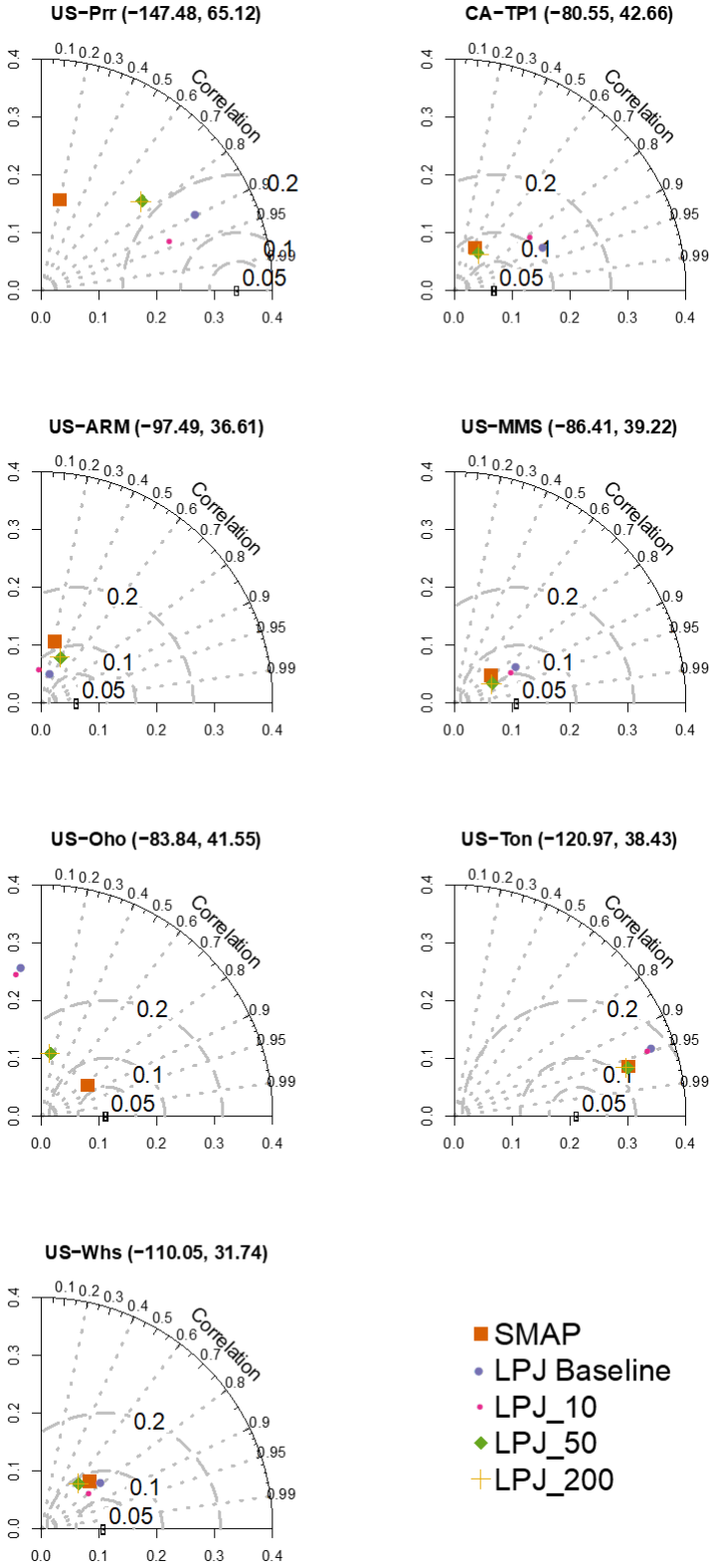

Figure 2. Taylor plots of monthly mean soil moisture in the 0–10 cm layer by assimilation schemes for all 7 sites. The cosine of the angle from the x axis is the correlation coefficient between simulated and observed soil moisture, which measures how well the simulated soil moisture captures the phasing and timing of the observed soil moisture from in situ sites. The black dots on the x axis represent observations. The radial distance from the origin is the standard deviation. The dotted and dashed grey lines represent correlation and RMSD normalized by standard deviation, respectively. The star symbol indicates a perfect model that has a zero RMSD and a correlation of 1.0.

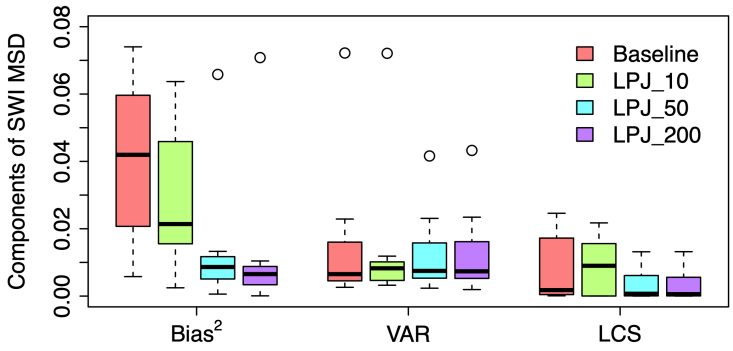

Figure 3. Boxplots showing the decomposed MSD for simulated monthly SWI from different assimilation schemes against the FLUXNET sites. The dots represent the outliers from the boreal site US-Prr, where SMAP has large discrepancies with the FLUXNET measurements.

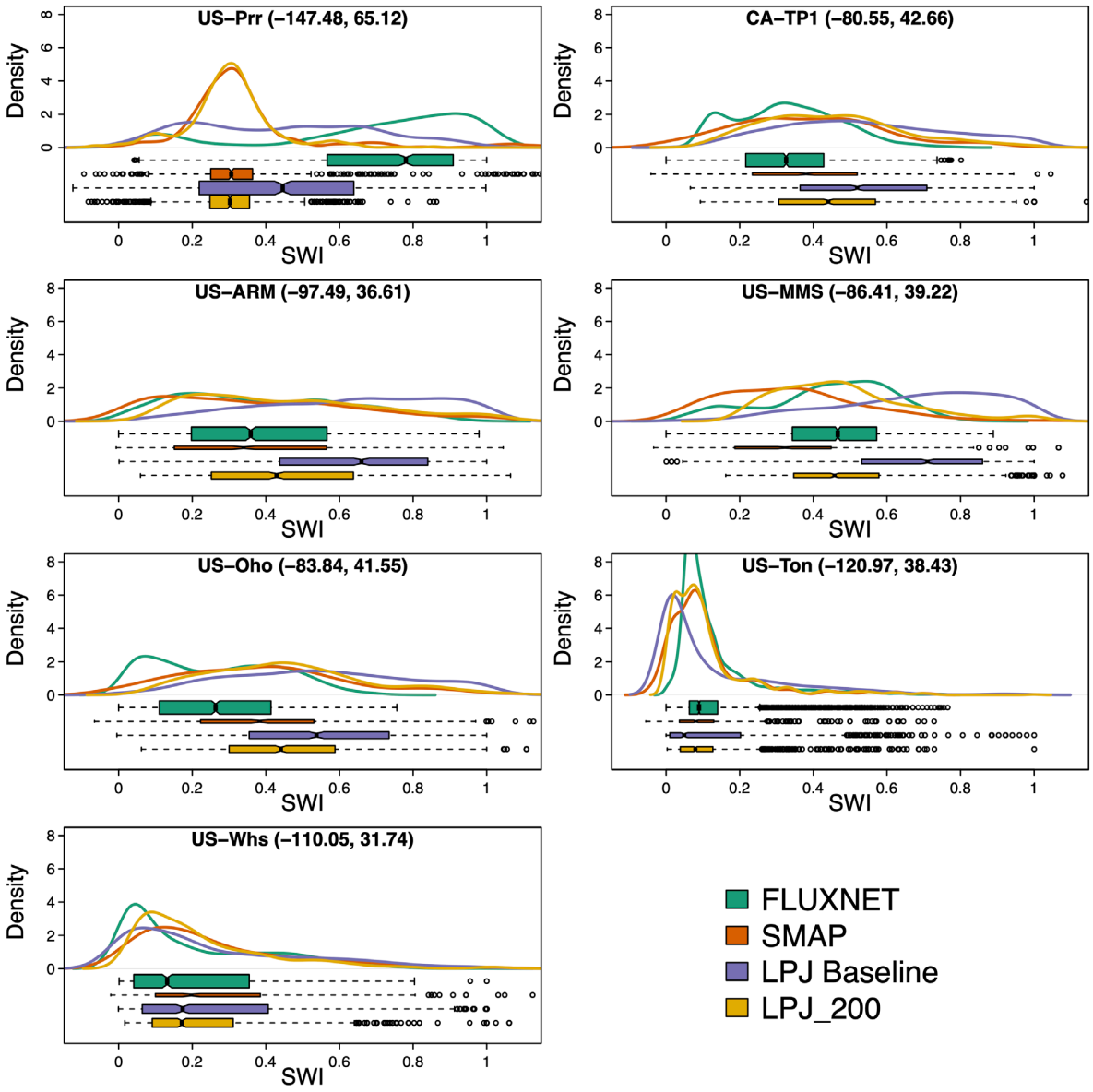

Figure 4. Distribution of simulated daily soil wetness index from baseline and assimilated run with FLUXNET and SMAP at the seven sites. The upper part and lower part of individual plots show the density distribution and box plot, respectively. The variable width of bars in the box plots corresponds to the sample size, with a wider bar indicating higher sample size.

The evaluation of the mean seasonal cycle of soil wetness in the simulations (versus that of FLUXNET measurements) suggested diverse patterns among sites and better agreement between the assimilation run and FLUXNET than was seen for the baseline (Figure 5). The improvement was more significant for the biomes that were less influenced by the freeze/thaw cycle and dense vegetation canopies. For the high-latitude site (US-Prr), both simulations captured well the onset and termination of the freeze/thaw cycle and produced a lower peak growing season compared to FLUXNET, with the assimilation run producing even lower soil moisture due to the weak seasonality captured by SMAP. For temperate forest sites (CA-TP1, US-MMS, and US-Oho), the assimilation run had a generally better agreement with FLUXNET, capturing the timing fairly well with improved peak and phase compared to the baseline run. The good agreements for US-Ton and US-Whs suggest there was less discrepancy between the model and the observations for the biomes that had open-canopy vegetations, where the assimilation run slightly improved the agreements with FLUXNET due to the higher accuracy of SMAP in these regions.

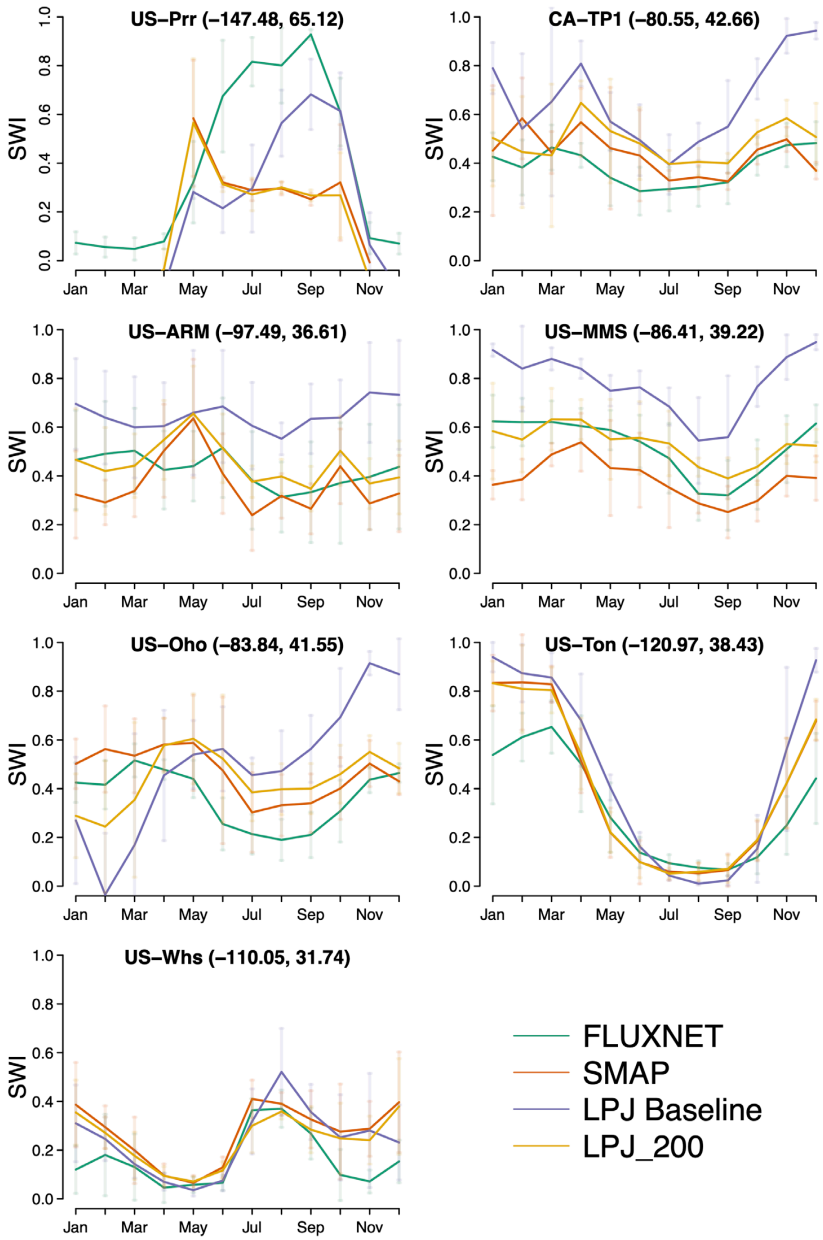

Figure 5. Mean seasonal cycle of soil wetness index for LPJ-wsl simulations, FLUXNET observations, and SMAP estimates for the seven sites. Error bars represent the range of one standard deviation.

3.3. Effect of Assimilation on Carbon Fluxes

Generally, for sites that have considerable discrepancies in soil moisture, the SMAP assimilation improved the agreement of seasonality in the net ecosystem CO_2 exchange with the FLUXNET observations (Figure 6). The assimilation of SMAP slightly altered the simulated CO_2 flux during the growing season, but had a limited effect on the seasonal pattern, despite significant changes in soil moisture for a few sites (e.g., US-Prr and CA-CP1). For the sites where the probability density function of modeled soil moisture agreed relatively well with SMAP (Figure 4; S-Ton and US-Whs), the assimilation resulted in a higher carbon uptake during the growing season but had a slightly weaker correlation with FLUXNET observations, suggesting that factors other than soil moisture likely control CO_2 flux during the growing season.

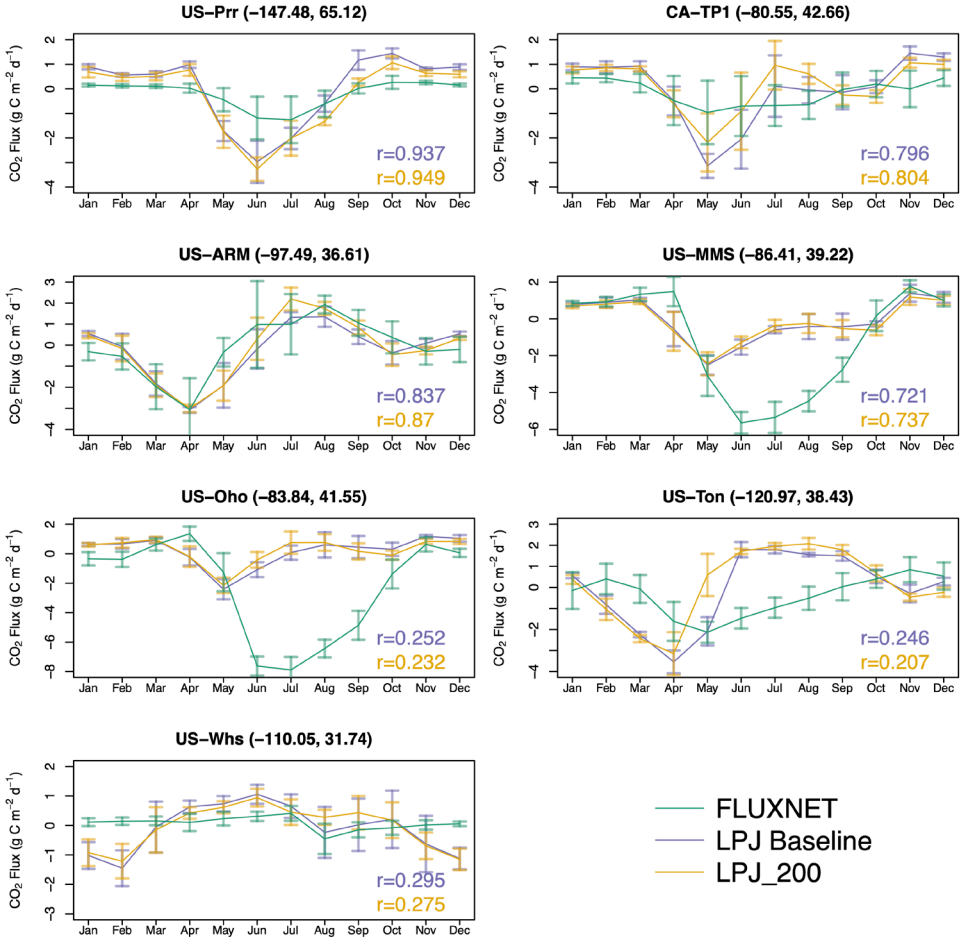

Figure 6. Mean seasonal cycle of simulated average monthly net ecosystem CO_2 exchange (NEE) from LPJ baseline and LPJ_200 in comparison with the FLUXNET sites. Error bar indicates standard deviation for multi-year NEE. The correlation coefficient between simulated NEE and FLUXNET observations are listed (purple: LPJ baseline; blue: LPJ_200).

To assess the effect of the assimilation of soil moisture on carbon fluxes at different time scales, we calculated the wavelet spectral of normalized residual errors between modeled carbon fluxes and FLUXNET measurement on the basis of site year (Figure 7). To improve the representativeness for biomes, 26 FLUXNET sites where SMAP observations were available and assimilated into LPJ-wsl were used to make the comparison. For each site year (2015–2019) from the LPJ-wsl simulation, the mean marginal distribution of the power spectrum showed the variations of model error with time scales. In this context, any time scales for which the model had lower power indicated improvements against the observations. This showed, for example, that the error in CO_2 flux in the model was

generally lowest at the monthly time scale (30 days) and higher at the shorter and longer time scales. This was reflected partly because of using the monthly climate datasets, as the sub-monthly simulations were based on a weather generator.

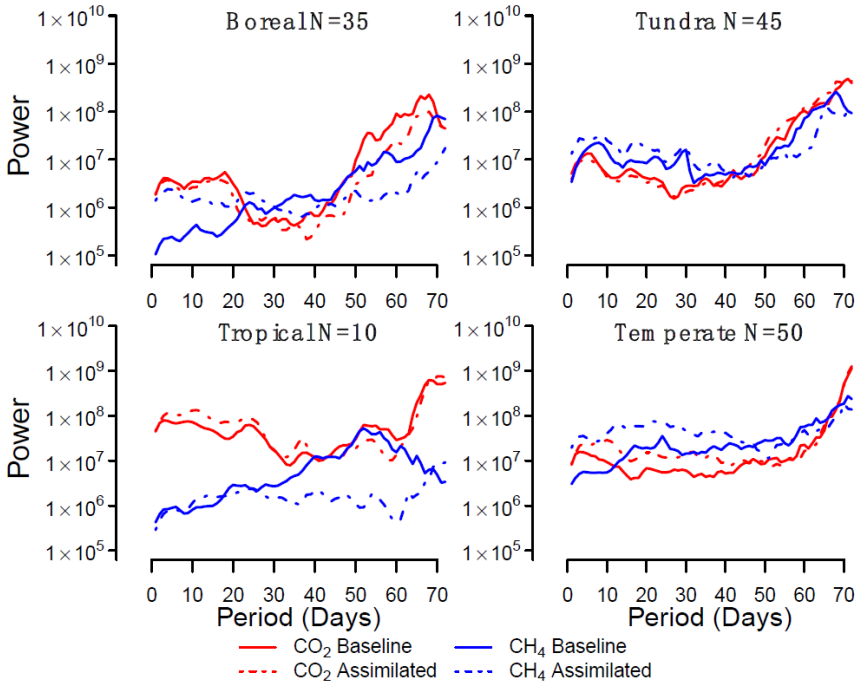

Figure 7. Mean marginal distribution of power spectra of the normalized residual error between modeled carbon fluxes and observations from FLUXNET sites. The higher power at specific time scales (period) indicates that the model error has a significantly higher mismatch at certain time scales. Sample sizes of site year for each biome are listed.

The comparison between the baseline and the assimilation run suggested improved agreement at time scales greater than 40 days for the boreal and tropical sites, with little/no improvement for the tundra and temperate sites. However, the assimilation run tended to have higher bias for time scales less than 30 days, which was partly due to the simple assimilation strategy that corrected the soil moisture every 3–5 days given the revisit time of SMAP. This assimilation strategy could possibly introduce unrealistic variability at these time scales, due to misaligned SMAP sampling meteorology with the weather generator in LPJ-wsl. Note that the site observations have large uncertainties in carbon fluxes with high year-to-year variations, especially for CH_4 observations, which are sensitive to environmental conditions such as water table depth and microbial composition [36,64,71]. The lack of measurements limits the evaluation for the tropical sites since only two subtropical grassland sites are available while no representation of tropical floodplain is included. In addition, the sites with CH_4 flux measurements tend to have high soil organic matter and saturated soil water; thus, the evaluation of assimilated CH_4 is affected by the accuracy of SMAP retrieval [73,75].

3.4. Evaluation of the Assimilation at Global Scale

To assess the effect of soil moisture assimilation at a global scale, we calculated the correlation coefficients and RMSD of the simulated daily soil moisture from the baseline and assimilated the run against SMAP and against the satellite-based surface soil moisture retrievals from the ESA CCI SM dataset for 2015–2019 (Figure 8). The results showed that LPJ-wsl baseline produced different temporal patterns than SMAP for the high latitudes and had a higher RMSD for most regions, except semi-arid regions, which is consistent with previous studies [74,76]. This was also the case for the metrics computed versus ESA CCI, which suggested a systematic difference between the satellite and model data,

with the highest agreement for semi-arid regions. As expected, the correlation and RMSD were improved (by construction) between the assimilation run and SMAP. The comparison with ESA CCI suggested that the assimilation could significantly increase the correlation coefficient and lower the RMSD for the northern high latitudes. Given that ESA CCI is an independent product, the reduced RMSD over large regions against the ESA CCI estimate indicates that the behavior of the model soil moisture is largely adjusted to be more consistent with satellite-based observations.

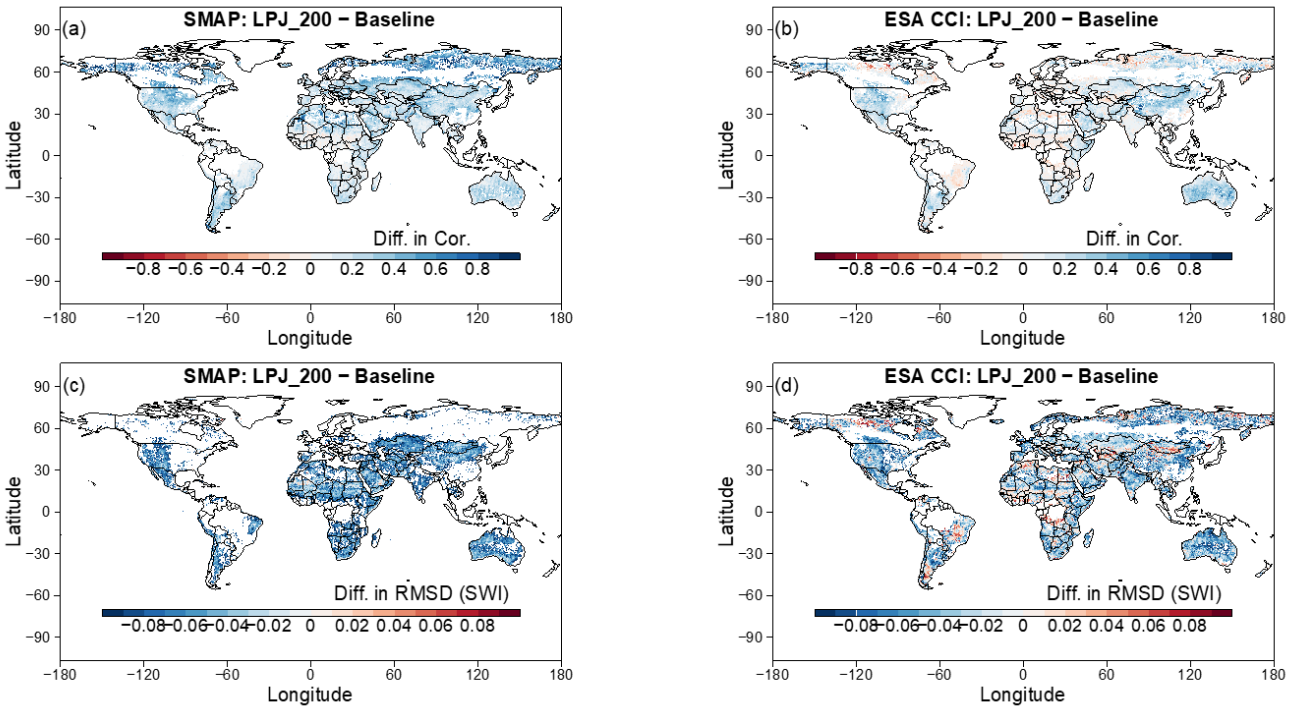

Figure 8. Difference in correlation coefficient (**a**,**b**) and RMSD (**c**,**d**) of simulated daily SWI between LPJ_200 and baseline when compared to two satellite soil moisture datasets (SMAP and ESA CCI) for 2015–2019. SMAP data were assimilated into LPJ_200. Blue color suggests improved agreement of LPJ-simulated SWI against the satellite datasets with the darker color representing higher agreements, while the red color represents reduced agreements.

3.5. Implications of Assimilated Results for Carbon Cycle Science

Even though, for many regions (e.g., tropical forests, high latitudes), SMAP observations are unavailable or have a very limited number of samples, it is still feasible to assess the influence of assimilating SMAP soil moisture at a regional scale. Below, we use two examples to demonstrate its potential influences on estimating carbon fluxes.

3.5.1. European Drought in 2018

Europe was stricken by an extreme summer heat wave and drought in 2018, which resulted in strong reductions in vegetation productivity and increased ecosystem respiration due to soil moisture deficits and, consequently, a reduction in the net CO_2 uptake in ecosystems [77]. Previous studies [78–80] have shown that prognostic land surface models tend to underestimate the effect of droughts due to the limited representation of hydrologic processes, which affects the simulated carbon balance through soil moisture deficits, high water vapor pressure, and heat stress.

Figure 9 shows that assimilating SMAP moisture into LPJ-wsl can introduce an improved seasonality in the net carbon uptake. Figure 9a shows that, despite both the baseline and assimilation runs showing good agreement, that there was a minimum in the soil moisture during the growing season, and assimilating SMAP reduced the amplitude of the seasonal cycle, with drier conditions during the non-growing seasons for 2015–2019.

It should also be noted that, even though the baseline simulated the extreme drought condition in 2018 reasonably well given the precipitation input from the observation-based climate datasets, SMAP suggested a less distinctive drought feature with higher 2018 summer soil moisture compared to the baseline.

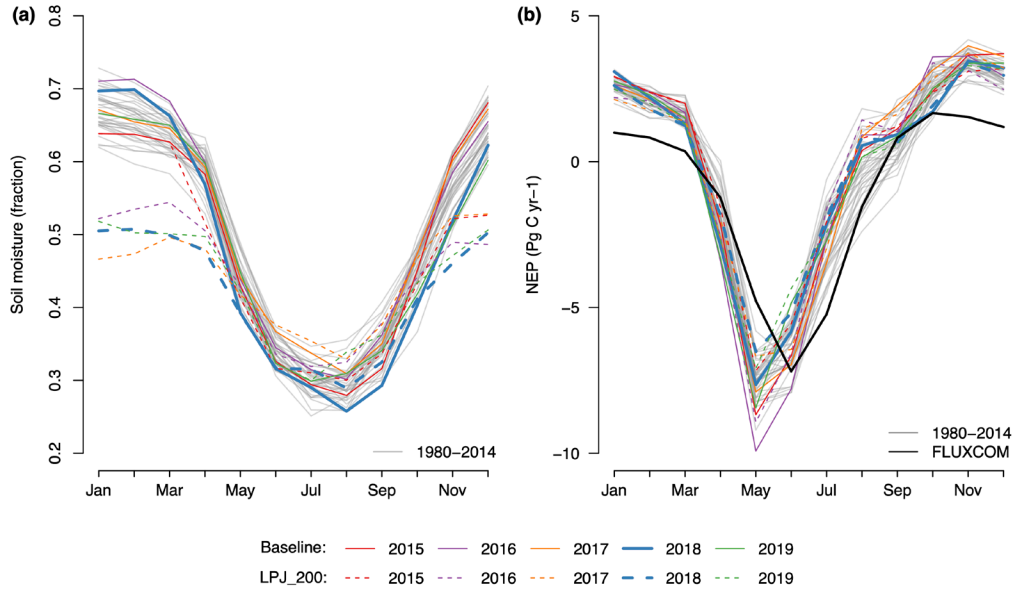

Figure 9. Influence of assimilation on net ecosystem productivity in continental Europe (32°N–75°N, 11°E–65°E). Seasonal cycles for 2015–2019 of LPJ-wsl estimates for (**a**) soil moisture and (**b**) net ecosystem productivity (NEP; negative values represent carbon uptake). For each year, the trajectories from the baseline (solid lines) and assimilation run (dashed lines) are shown with matching colors. The estimated average seasonality from FLUXCOM is for 2001–2010.

The seasonal cycle of net ecosystem productivity reveals important differences between the baseline and assimilation runs in estimating carbon fluxes (Figure 9b). The assimilation run shows that SMAP produced extremely low peak carbon uptake during the summer of 2018, while the baseline run suggests a moderate drought effect on net carbon uptake. Considering that SMAP introduces a wetter soil condition during the growing season than the baseline, this indicates the significant influence of soil moisture during the early growing season, when the drier soil conditions introduced by SMAP had a weak impact on vegetation growth during the early growing season but had a strong influence on evapotranspiration (Figure A2). The less affected vegetation growth contributes to a high soil moisture depletion during the growing season, which amplifies the overall effect of summer droughts on net ecosystem productivity (Figure A2). This resulted in a weak net annual carbon source of 0.07 Pg C yr^{-1} in 2018, in contrast to a net annual carbon uptake (sink) of −0.17 Pg C yr^{-1} from the baseline. In addition, the assimilation can produce a lower seasonality in net carbon uptake during the growing season, which is in better agreement with FLUXCOM.

3.5.2. Sudd Wetlands

Assimilated soil moisture has been shown to improve the spatio-temporal distribution of modeled CH_4 fluxes over the South Sudan region, with a central focus on the Sudd wetlands. We chose the Sudd wetlands because of their important role in wetland CH_4 emissions highlighted by recent studies [81–83], as well as the good accuracy and spatial coverage of SMAP soil moisture for the low-canopy-density region [74]. The map of difference in soil moisture between the assimilation run and baseline clearly shows that the assimilation run produced higher soil moisture around the Sudd wetland regions, causing higher estimates of wetland area due to higher water table depth through the TOPMODEL hydrologic module of LPJ-wsl. The higher wetland areas estimated by the assimilation run

were consistent with the findings from [83], which suggests that wetland models largely underestimate the wetland area of the Sudd region.

The modeled CH_4 fluxes over the Sudd wetlands from the assimilation run had better agreement in terms of their seasonal cycle and annual total with posterior estimates from the inversion models [81,83] based on satellite measurements (Figure 10). The assimilation run showed a dual peak of CH_4 fluxes in the March–April–May and September–October–November seasons, which is consistent with the seasonality detected by inversion models based on GOSAT and TROPOMI measurements [81,82]. In contrast, the baseline generally produces a lower intra-seasonal variability than the assimilation run, with the highest emissions in the late growing season. In addition, the timing of a record high peak in SON 2019 is consistent with the posterior estimates based on TROPOMI measurements [82], which suggests a strong positive anomaly of CH_4 flux due to an exceptional rainfall event. The average annual total flux for 2015–2019 almost doubled from 2.4 Tg CH_4 yr^{-1} at the baseline to 4.4 Tg CH_4 yr^{-1} in the assimilation run, which can be explained by a potential underestimation of the wetland area in the baseline run. The mean annual total flux in 2018–2019 from the assimilation run was 4.7 Tg CH_4 yr^{-1}, which falls into the range of 7.3 $\pm$ 3.2 Tg yr^{-1} from [83] based on TROPOMI measurements, but is higher than the 3.4 $\pm$ 0.3 Tg CH_4 yr^{-1} estimate from [82] based on TROPOMI and GOSAT measurements.

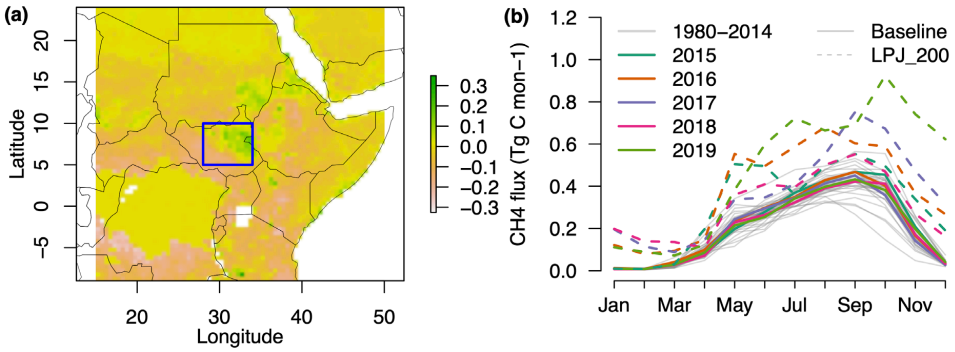

Figure 10. Influence of assimilation on CH_4 fluxes over South Sudan's wetlands. (**a**) Spatial distribution of difference of annual mean soil moisture between assimilation and baseline (LPJ_200 minus baseline) over 2015–2019 for the South Sudan region. The area within the blue rectangle (5°N–10°N, 28°E–35°E) is referred to as the Sudd wetland region. (**b**) Seasonal cycle of wetland CH_4 fluxes for the Sudd wetland region.

4. Discussion

Throughout this paper, we assessed the potential of the SMAP soil moisture product to be used to improve the LPJ-wsl simulation of carbon fluxes. Because systematic errors exist in both the SMAP product and the process-based models, the climatological rescaling of soil moisture between SMAP and LPJ-wsl is essential. The SWI conversion approach in this study has been proven to be useful at inducing the seasonality of soil moisture dynamics [84,85]. Given that it is difficult to adjust the model formulation, soil hydraulic characterization, and the degree of wetness relative to the range of moisture over which key processes (drainage, evapotranspiration) occur, the potential bias in the SWI conversion in this study and its effect on assimilation needs further investigation. A better rescaling approach for SMAP is needed to keep both sources relatively consistent, such as the linear cumulative density distribution (CDF) matching or the full CDF matching [26,60]. In addition, because the SMAP descending retrievals at local time (6 a.m.) were applied in this study, a proper conversion of SMAP soil moisture to daily averages may need to be developed to minimize the mismatch with the modeled daily average soil moisture.

The simulation experiments with different representative depths demonstrate the importance of assessing the suitable depth to be considered in the assimilation. Despite the fact that LPJ-wsl is discretized by an eight-layered hydrology scheme, there is no exact corresponding depth to match the thin surface layer detected by the SMAP instrument.

In addition, the sensing depth of SMAP is affected by local environmental conditions and vegetation types [75]. Therefore, it is impossible to fully reconcile the discrepancies in modeled soil moisture with remotely sensed measurements, as there is a structural mismatch between satellite-based observations and terrestrial ecosystem models. In this study, we tested altering the soil moisture using a first-order method by replacing the soil moisture with observations for a specific depth. A better approach to improve the issue of representativeness is to use an exponential filter [86–88], which assumes that the soil moisture of deeper layers can be derived from an exponential relationship given the observed soil moisture in the surface layer.

The improvement of the assimilation over different regions largely depended on the agreement of SMAP with the in situ measurements. This is reflected in the comparison between the model and the data, which highlighted that the model behavior with respect to soil moisture after assimilation had high similarity in a spatio-temporal pattern with SMAP, despite the simulated carbon fluxes that are still subject to the model structure, forcing errors, and parameter errors. This indicates that, globally, the assimilation does not necessarily yield better agreement with upscaled carbon flux products. This is possibly due to the limited accuracy of SMAP for regions with dense vegetation or high soil organic matter, given the influence of vegetation water content on the canopy in terms of the retrieval of soil moisture at the surface [89] and the underrepresentation of soil organic matter in radiative transfer modeling [90]. It is also worth noting that it is difficult to evaluate the spatial patterns of carbon fluxes with the upscaling products, which are also affected by the spatial distribution of sites, where regions with little/no representativeness tend to have higher bias in carbon fluxes, e.g., in the tropics [67].

Nevertheless, our result, showing that SMAP soil moisture can be used to represent deeper layers than 5 cm, was expected based on previous studies. Namely, under drier conditions, the emission depth of L-band microwaves greatly increases beyond 5 cm. Under wetter conditions, L-band soil moisture has a greater information content of deeper soil layers [56,57]. It is unexpected that SMAP would best represent moisture dynamics in the full 200 cm LPJ soil column. We speculate that this results from the fact that LPJ's simple representation of infiltration to deeper soil layers may not capture monthly and seasonal dynamics. SMAP may provide a first-order constraint on the deeper soil layer dynamics. It is possible that the best performance may come from an improved LPJ representation of deeper soil moisture dynamics between 50 and 200 cm, along with SMAP assimilated into the top 50 cm layer. Alternatively, future LPJ representations can consider assimilating GRACE terrestrial water storage dynamics for the deepest soil layers.

The evaluation of simulated carbon fluxes against FLUXNET is inherently limited by the sparse spatial observations and the nature of high site-to-site variability. Owing to the very sparse coverage of the FLUXNET sites (n = 26) applied in the wavelet analysis, there is still large uncertainty and potential bias in the analysis that needs to be further investigated. Because of the purpose of evaluating CO_2 and CH_4 fluxes simultaneously, the selected sites tended to have high soil moisture and soil organic matter. This influences the accuracy of SMAP retrievals as the dielectric mixing model in SMAP does not explicitly consider organic matter or the potential bias of SMAP in high soil wetness conditions [75,89]. In addition, errors in the surface meteorological forcing may explain the differences between the model estimate and the SMAP product, as most of the variability of soil moisture is driven by precipitation events [91]. Therefore, the evaluation metrics are affected by the forcing errors, especially since the gridded climate dataset (i.e., CRU) applied in LPJ-wsl simulation is different from the in situ meteorological conditions.

The promising but limited improvements in modeled carbon fluxes after the first-order assimilation in this study show that more sophisticated assimilation approaches are needed. A thorough examination of the bias in simulated soil moisture would help to isolate the bias induced by parameterization and unmodeled processes from the total systematic difference between the model and observations, which was treated as bias in this study. This is the prerequisite to employ more sophisticated assimilation approaches such as the ensemble Kalman

filter [92]. To improve the simulated carbon fluxes at a sub-monthly scale, a few temporal gap-filling approaches (e.g., SWI smoothing filter) are useful to potentially improve the soil moisture at a sub-monthly scale. Lastly, given that soil moisture can influence multiple components of the carbon cycle processes in terrestrial ecosystem models, it is better to use multiple independent constraints in the data assimilation, as proven by previous studies [30,32]. A further principal component analysis is needed to examine the best combination of constraining parameters with SMAP to determine the multiple-constraint assimilation scheme either by a stepwise approach [93] or by a simultaneous approach [30].

The improved estimates of CO_2 and CH_4 fluxes after assimilation at regional scale suggest important implications of assimilating SMAP soil moisture into terrestrial ecosystem models for carbon cycle research. The assimilation of SMAP can help explain the response of terrestrial ecosystems to climate events. As the simulations for the 2018 European extreme drought suggested, the assimilated spatio-temporal patterns of soil moisture could result in strong reductions in vegetation productivity during the onset of drought events and cause a strong legacy effect in the subsequent vegetation mortality, yielding a significant impact on the net carbon uptake. Assimilating SMAP soil moisture also shows capacity in capturing pulses of wetland CH_4 emissions for regions that do not have reliable direct measurements. The spatio-temporal distribution of wetland CH_4 in Sudd wetlands corroborates the underestimated wetland CH_4 emission in that region detected by the TROPOMI measurements [82], as well as a few recent atmospheric inversion results [81,82]. Note that improving soil moisture has a limited effect. An example is that TROPOMI detected high emission in the December–January–February (DJF) season for the Sudd wetland, whereas for both the baseline and assimilation runs the inundated area was lowest. This can be explained by model structure: the model is mainly driven by precipitation, which is suggested to be lowest in the DJF season, while river height is at a high level. This is a feasible way to incorporate the advantages of SMAP to assess the effect of soil moisture on the terrestrial carbon cycle given its unique role in directly monitoring the surface condition continuously.

5. Conclusions

Even though there have been many studies evaluating the usefulness of the SMAP dataset for land surface modeling, this study provides the first experiment at a global scale that evaluates the effect of SMAP soil moisture on simulated CO_2 and CH_4 fluxes. Through a direct insertion method, we found that assimilating SMAP can produce a modest improvement in soil moisture against site-level observations with altered seasonal dynamics. The assimilated run showed a promising but limited improvement over site-level CO_2 and CH_4 fluxes at long time scales (>40 days) for boreal and tropical sites, with little/no improvement for the tundra and temperate sites. The assessment of the assimilating run for two climatic events at a regional scale suggested that SMAP can help the model to capture the observed seasonality of CO_2 and CH_4 fluxes. The work presented here confronts how well the model can capture the temporal pattern of soil moisture and prompts future analysis to utilize SMAP in simulating coupling between soil moisture and carbon fluxes.

Author Contributions: Conceptualization, Z.Z., A.C. and B.P.; Data curation, Z.Z.; Formal analysis, Z.Z.; Funding acquisition, A.C. and B.P.; Investigation, L.O., R.R. and A.F.F.; Project administration, L.O.; Writing—original draft, Z.Z.; Writing—review & editing, Z.Z., A.C., L.O., R.R., A.F.F. and B.P. All authors have read and agreed to the published version of the manuscript.

Funding: This research was funded by the NASA SUSMAP grant under Cooperative Agreement Number NNX16AQ22G. Z. Zhang was supported by the NASA Research Grant and Cooperative Agreement 80NSSC20K0731. R. Reichle was supported by the NASA SMAP mission.

Data Availability Statement: SMAP Level3 soil moisture data are available from the National Snow and Ice Data Center following registration. The eddy covariance observations from the FLUXNET and FLUXNET-CH4 dataset can be downloaded at https://fluxnet.fluxdata.org/ (accessed on 12 September 2021) and https://fluxnet.org/data/fluxnet-ch4-community-product (accessed on 12 September 2021).

Acknowledgments: We thank Alka Singh for sharing the processed SMAP Level 3 soil moisture dataset. We gratefully acknowledge the eddy covariance data acquired and shared by the FLUXNET community.

Conflicts of Interest: The authors declare no conflict of interest.

Appendix A

Appendix A.1. Wavelet Analysis

Figure A1 show an example of how the marginal distribution of power spectra is calculated. First, we use the time series of model and observation for each site-year to calculate the normalized residual error. Second, we tested data-model agreement in the frequency domain for CO_2 and CH_4 fluxes by calculating the spectral properties of the daily times series of normalized residual error in CO_2 and CH_4 fluxes. At the last we calculate marginal distribution of spectra of the normalized residual errors grouped by site biomes.

Table A1. List of sites from FLUXNET for carbon fluxes evaluations. Descriptions about the site can be found via Site ID at https://fluxnet.org/sites/site-summary/ (accessed on 19 February 2021).

Biome	Site ID
Boreal	FI-LOM; RU-CH2; RU-HE; US-BZB; US-BZS; US-NGC; US-UAF
Tundra	RU-COK; RU-SAM; RU-VRK; SE-ST1; SE-STO; US-A03; US-A10; US-ATQ; US-BEO; US-BES; US-BRW; US-EML; US-ICS; US-IVO; US-NGB
Temperate	CH-DAV; DE-DGW; DE-ZRK; FR-LGT; IT-CAS; MA-ERC; UK-LBT; US-BI1; US-BI2; US-CRT; US-TW3;
Tropical	US-DPW; US-LA1; US-LA2;

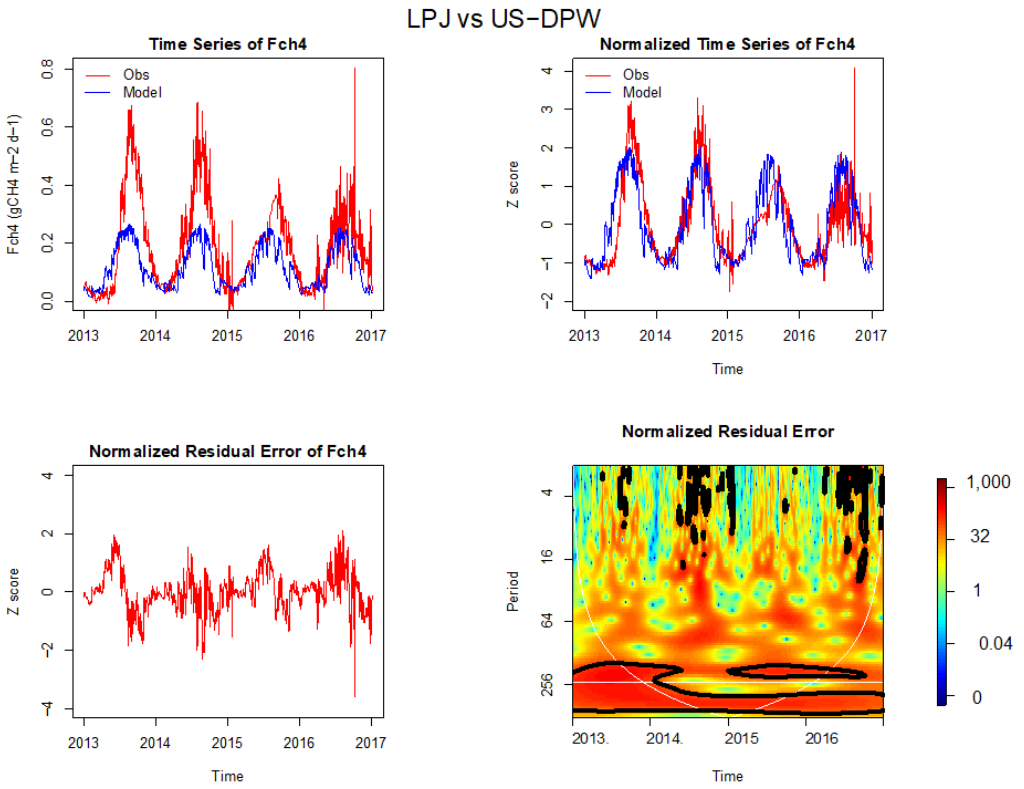

Figure A1. An example of the processing of wavelet analysis for CH_4 fluxes in one site US-DPW v.s. LPJ-wsl.

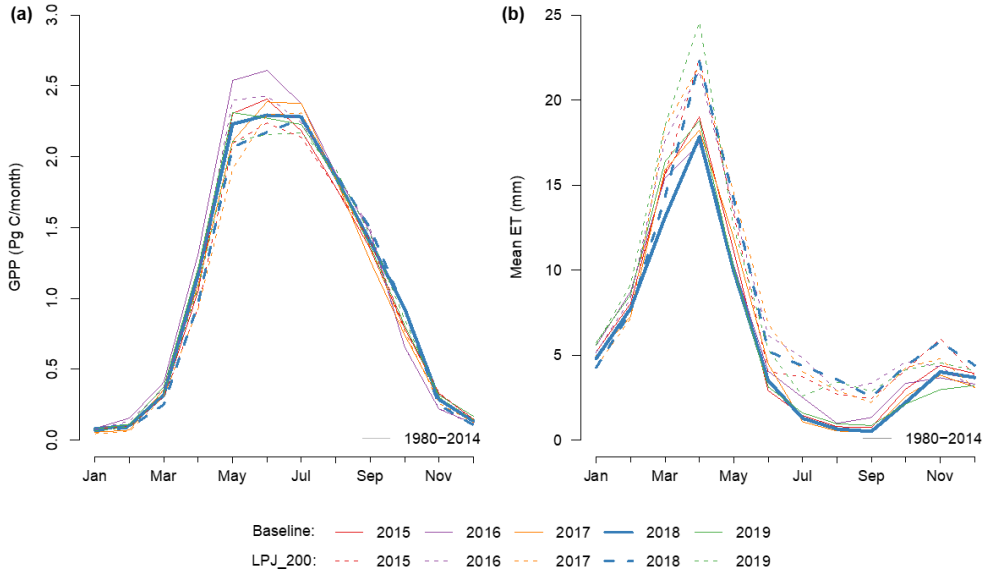

Figure A2. Seasonal cycles for 2015–2019 of LPJ-wsl estimates for (**a**) Gross Primary Production (GPP) and (**b**) mean evapotranspiration (ET). For each year, the trajectories from the baseline (solid lines) and assimilation run (dashed lines) are shown with matching colors.

References

1. Green, J.K.; Seneviratne, S.I.; Berg, A.M.; Findell, K.L.; Hagemann, S.; Lawrence, D.M.; Gentine, P. Large influence of soil moisture on long-term terrestrial carbon uptake. *Nature* **2019**, *565*, 476–479. [CrossRef] [PubMed]
2. Zhao, M.; Running, S.W. Drought-Induced Reduction in Global Terrestrial Net Primary Production from 2000 through 2009. *Science* **2010**, *329*, 940–943. [CrossRef] [PubMed]
3. Liu, L.; Gudmundsson, L.; Hauser, M.; Qin, D.; Li, S.; Seneviratne, S.I. Soil moisture dominates dryness stress on ecosystem production globally. *Nat. Commun.* **2020**, *11*, 4892. [CrossRef] [PubMed]
4. Humphrey, V.; Zscheischler, J.; Ciais, P.; Gudmundsson, L.; Sitch, S.; Seneviratne, S.I. Sensitivity of atmospheric CO_2 growth rate to observed changes in terrestrial water storage. *Nature* **2018**, *560*, 628–631. [CrossRef]
5. Fan, Y.; Miguez-Macho, G. A simple hydrologic framework for simulating wetlands in climate and earth system models. *Clim. Dyn.* **2011**, *37*, 253–278. [CrossRef]
6. Cosby, B.J.; Hornberger, G.M.; Clapp, R.B.; Ginn, T.R. A Statistical Exploration of the Relationships of Soil Moisture Characteristics to the Physical Properties of Soils. *Water Resour. Res.* **1984**, *20*, 682–690. [CrossRef]
7. Koster, R.D.; Guo, Z.; Yang, R.; Dirmeyer, P.A.; Mitchell, K.; Puma, M.J. On the Nature of Soil Moisture in Land Surface Models. *J. Clim.* **2009**, *22*, 4322–4335. [CrossRef]
8. Ahlström, A.; Xia, J.; Arneth, A.; Luo, Y.; Smith, B. Importance of vegetation dynamics for future terrestrial carbon cycling. *Environ. Res. Lett.* **2015**, *10*, 054019. [CrossRef]
9. Poulter, B.; Frank, D.; Ciais, P.; Myneni, R.B.; Andela, N.; Bi, J.; Broquet, G.; Canadell, J.G.; Chevallier, F.; Liu, Y.Y.; et al. Contribution of semi-arid ecosystems to interannual variability of the global carbon cycle. *Nature* **2014**, *509*, 600–603. [CrossRef]
10. Rodell, M.; Famiglietti, J.S.; Wiese, D.N.; Reager, J.T.; Beaudoing, H.K.; Landerer, F.W.; Lo, M.-H. Emerging trends in global freshwater availability. *Nature* **2018**, *557*, 651–659. [CrossRef]
11. dos Santos, T.; Keppel-Aleks, G.; De Roo, R.; Steiner, A.L. Can Land Surface Models Capture the Observed Soil Moisture Control of Water and Carbon Fluxes in Temperate-to-Boreal Forests? *J. Geophys. Res. Biogeosci.* **2021**, *126*, e2020JG005999. [CrossRef]
12. Booth, E.G.; Loheide, S.P., II. Hydroecological model predictions indicate wetter and more diverse soil water regimes and vegetation types following floodplain restoration. *J. Geophys. Res. Biogeosci.* **2012**, *117*, G02011. [CrossRef]
13. Knorr, W.; Heimann, M. Uncertainties in global terrestrial biosphere modeling: 1. A comprehensive sensitivity analysis with a new photosynthesis and energy balance scheme. *Glob. Biogeochem. Cycles* **2001**, *15*, 207–225. [CrossRef]
14. Zaehle, S.; Sitch, S.; Smith, B.; Hatterman, F. Effects of parameter uncertainties on the modeling of terrestrial biosphere dynamics: Parameter-Based Uncertainty of a Dgvm. *Glob. Biogeochem. Cycles* **2005**, *19*, GB3020. [CrossRef]
15. Babaeian, E.; Sadeghi, M.; Jones, S.B.; Montzka, C.; Vereecken, H.; Tuller, M. Ground, Proximal, and Satellite Remote Sensing of Soil Moisture. *Rev. Geophys.* **2019**, *57*, 530–616. [CrossRef]
16. Chan, S.K.; Bindlish, R.; O'Neill, P.E.; Njoku, E.; Jackson, T.; Colliander, A.; Chen, F.; Burgin, M.; Dunbar, S.; Piepmeier, J.; et al. Assessment of the SMAP Passive Soil Moisture Product. *IEEE Trans. Geosci. Remote Sens.* **2016**, *54*, 4994–5007. [CrossRef]

17. Fernandez-Moran, R.; Al-Yaari, A.; Mialon, A.; Mahmoodi, A.; Al Bitar, A.; de Lannoy, G.; Rodriguez-Fernandez, N.; Lopez-Baeza, E.; Kerr, Y.; Wigneron, J.-P. SMOS-IC: An Alternative SMOS Soil Moisture and Vegetation Optical Depth Product. *Remote Sens.* **2017**, *9*, 457. [CrossRef]
18. Kerr, Y.H.; Al-Yaari, A.; Rodriguez-Fernandez, N.; Parrens, M.; Molero, B.; Leroux, D.; Bircher, S.; Mahmoodi, A.; Mialon, A.; Richaume, P.; et al. Overview of SMOS performance in terms of global soil moisture monitoring after six years in operation. *Remote Sens. Environ.* **2016**, *180*, 40–63. [CrossRef]
19. Parinussa, R.M.; Holmes, T.R.H.; Wanders, N.; Dorigo, W.A.; de Jeu, R.A.M. A Preliminary Study toward Consistent Soil Moisture from AMSR2. *J. Hydrometeorol.* **2015**, *16*, 932–947. [CrossRef]
20. Wagner, W.; Hahn, S.; Kidd, R.; Melzer, T.; Bartalis, Z.; Hasenauer, S.; Figa-Saldaña, J.; de Rosnay, P.; Jann, A.; Schneider, S.; et al. The ASCAT Soil Moisture Product: A Review of its Specifications, Validation Results, and Emerging Applications. *Meteorol. Z.* **2013**, *22*, 5–33. [CrossRef]
21. Kerr, Y.H.; Waldteufel, P.; Wigneron, J.; Delwart, S.; Cabot, F.; Boutin, J.; Escorihuela, M.; Font, J.; Reul, N.; Gruhier, C.; et al. The SMOS Mission: New Tool for Monitoring Key Elements ofthe Global Water Cycle. *Proc. IEEE* **2010**, *98*, 666–687. [CrossRef]
22. Entekhabi, D.; Njoku, E.G.; O'Neill, P.E.; Kellogg, K.H.; Crow, W.T.; Edelstein, W.N.; Entin, J.K.; Goodman, S.D.; Jackson, T.J.; Johnson, J.; et al. The Soil Moisture Active Passive (SMAP) Mission. *Proc. IEEE* **2010**, *98*, 704–716. [CrossRef]
23. Wigneron, J.-P.; Jackson, T.J.; O'Neill, P.; de Lannoy, G.; de Rosnay, P.; Walker, J.P.; Ferrazzoli, P.; Mironov, V.; Bircher, S.; Grant, J.P.; et al. Modelling the passive microwave signature from land surfaces: A review of recent results and application to the L-band SMOS & SMAP soil moisture retrieval algorithms. *Remote Sens. Environ.* **2017**, *192*, 238–262. [CrossRef]
24. Beck, H.E.; Pan, M.; Miralles, D.G.; Reichle, R.H.; Dorigo, W.A.; Hahn, S.; Sheffield, J.; Karthikeyan, L.; Balsamo, G.; Parinussa, R.M.; et al. Evaluation of 18 satellite- and model-based soil moisture products using in situ measurements from 826 sensors. *Hydrol. Earth Syst. Sci.* **2021**, *25*, 17–40. [CrossRef]
25. Barbu, A.L.; Calvet, J.-C.; Mahfouf, J.-F.; Lafont, S. Integrating ASCAT surface soil moisture and GEOV1 leaf area index into the SURFEX modelling platform: A land data assimilation application over France. *Hydrol. Earth Syst. Sci.* **2014**, *18*, 173–192. [CrossRef]
26. de Lannoy, G.J.M.; Reichle, R.H. Assimilation of SMOS brightness temperatures or soil moisture retrievals into a land surface model. *Hydrol. Earth Syst. Sci.* **2016**, *20*, 4895–4911. [CrossRef]
27. Lievens, H.; Reichle, R.H.; Liu, Q.; de Lannoy, G.J.M.; Dunbar, R.S.; Kim, S.B.; Das, N.N.; Cosh, M.; Walker, J.P.; Wagner, W. Joint Sentinel-1 and SMAP data assimilation to improve soil moisture estimates. *Geophys. Res. Lett.* **2017**, *44*, 6145–6153. [CrossRef]
28. de Rosnay, P.; Drusch, M.; Vasiljevic, D.; Balsamo, G.; Albergel, C.; Isaksen, L. A simplified Extended Kalman Filter for the global operational soil moisture analysis at ECMWF. *Q. J. R. Meteorol. Soc.* **2013**, *139*, 1199–1213. [CrossRef]
29. Jones, L.A.; Kimball, J.S.; Reichle, R.H.; Madani, N.; Glassy, J.; Ardizzone, J.V.; Ardizzone, J.V.; Colliander, A.; Cleverly, J.; Desai, A.R.; et al. The SMAP Level 4 Carbon Product for Monitoring Ecosystem Land–Atmosphere CO_2 Exchange. *IEEE Trans. Geosci. Remote Sens.* **2017**, *55*, 6517–6532. [CrossRef]
30. Scholze, M.; Kaminski, T.; Knorr, W.; Blessing, S.; Vossbeck, M.; Grant, J.P.; Scipal, K. Simultaneous assimilation of SMOS soil moisture and atmospheric CO_2 in-situ observations to constrain the global terrestrial carbon cycle. *Remote Sens. Environ.* **2016**, *180*, 334–345. [CrossRef]
31. Rahman, A.; Zhang, X.; Xue, Y.; Houser, P.; Sauer, T.; Kumar, S.; Mocko, D.; Maggioni, V. A synthetic experiment to investigate the potential of assimilating LAI through direct insertion in a land surface model. *J. Hydrol. X* **2020**, *9*, 100063. [CrossRef]
32. Wu, M.; Scholze, M.; Kaminski, T.; Voßbeck, M.; Tagesson, T. Using SMOS soil moisture data combining CO_2 flask samples to constrain carbon fluxes during 2010–2015 within a Carbon Cycle Data Assimilation System (CCDAS). *Remote Sens. Environ.* **2020**, *240*, 111719. [CrossRef]
33. Sitch, S.; Smith, B.; Prentice, I.C.; Arneth, A.; Bondeau, A.; Cramer, W.; Kaplan, J.O.; Levis, S.; Lucht, W.; Sykes, M.T.; et al. Evaluation of ecosystem dynamics, plant geography and terrestrial carbon cycling in the LPJ dynamic global vegetation model. *Glob. Chang. Biol.* **2003**, *9*, 161–185. [CrossRef]
34. Zhang, Z.; Zimmermann, N.E.; Kaplan, J.O.; Poulter, B. Modeling spatiotemporal dynamics of global wetlands: Comprehensive evaluation of a new sub-grid TOPMODEL parameterization and uncertainties. *Biogeosciences* **2016**, *13*, 1387–1408. [CrossRef]
35. Pastorello, G.; Trotta, C.; Canfora, E.; Chu, H.; Christianson, D.; Cheah, Y.-W.; Poindexter, C.; Chen, J.; Elbashandy, A.; Humphrey, M.; et al. The FLUXNET2015 dataset and the ONEFlux processing pipeline for eddy covariance data. *Sci. Data* **2020**, *7*, 225. [CrossRef]
36. Delwiche, K.B.; Knox, S.H.; Malhotra, A.; Fluet-Chouinard, E.; McNicol, G.; Feron, S.; Ouyang, Z.; Papale, D.; Trotta, C.; Canfora, E.; et al. FLUXNET-CH_4: A global, multi-ecosystem dataset and analysis of methane seasonality from freshwater wetlands. *Earth Syst. Sci. Data* **2021**, *13*, 3607–3689. [CrossRef]
37. Katul, G.; Lai, C.-T.; Schäfer, K.; Vidakovic, B.; Albertson, J.; Ellsworth, D.; Oren, R. Multiscale analysis of vegetation surface fluxes: From seconds to years. *Adv. Water Resour.* **2001**, *24*, 1119–1132. [CrossRef]
38. Torrence, C.; Compo, G.P. A Practical Guide to Wavelet Analysis. *Bull. Am. Meteorol. Soc.* **1998**, *79*, 61–78. [CrossRef]
39. Gerten, D.; Schaphoff, S.; Haberlandt, U.; Lucht, W.; Sitch, S. Terrestrial vegetation and water balance—Hydrological evaluation of a dynamic global vegetation model. *J. Hydrol.* **2004**, *286*, 249–270. [CrossRef]
40. Wania, R.; Ross, I.; Prentice, I.C. Integrating peatlands and permafrost into a dynamic global vegetation model: 2. Evaluation and sensitivity of vegetation and carbon cycle processes. *Glob. Biogeochem. Cycles* **2009**, *23*, GB3015. [CrossRef]

41. Fischer, G.; Nachtergaele, F.; Prieler, S.; van Velthuizen, H.T.; Verelst, L.; Wiberg, D. *Global Agro-Ecological Zones Assessment for Agriculture (GAEZ 2008)*; IIASA: Italy, Austria; FAO: Rome, Italy, 2008.
42. Hodson, E.L.; Poulter, B.; Zimmermann, N.E.; Prigent, C.; Kaplan, J.O. The El Niño-Southern Oscillation and wetland methane interannual variability. *Geophys. Res. Lett.* **2011**, *38*, L08810. [CrossRef]
43. Pickett-Heaps, C.A.; Jacob, D.J.; Wecht, K.J.; Kort, E.A.; Wofsy, S.C.; Diskin, G.S.; Worthy, D.E.J.; Kaplan, J.O.; Bey, I.; Drevet, J. Magnitude and seasonality of wetland methane emissions from the Hudson Bay Lowlands (Canada). *Atmos. Chem. Phys.* **2011**, *11*, 3773–3779. [CrossRef]
44. Pangala, S.R.; Enrich-Prast, A.; Basso, L.S.; Peixoto, R.B.; Bastviken, D.; Hornibrook, E.R.C.; Gatti, L.V.; Marotta, H.; Calazans, L.S.B.; Sakuragui, C.M.; et al. Large emissions from floodplain trees close the Amazon methane budget. *Nature* **2017**, *552*, 230–234. [CrossRef] [PubMed]
45. Poulter, B.; Frank, D.C.; Hodson, E.L.; Zimmermann, N.E. Impacts of land cover and climate data selection on understanding terrestrial carbon dynamics and the CO_2 airborne fraction. *Biogeosciences* **2011**, *8*, 2027–2036. [CrossRef]
46. Sweeney, C.; Chatterjee, A.; Wolter, S.; McKain, K.; Bogue, R.; Newberger, T.; Hu, L.; Ott, L.; Poulter, B.; Schiferl, L.; et al. Atmospheric carbon cycle dynamics over the ABoVEdomain: An integrated analysis using aircraft observations (Arctic-CAP) and model simulations (GEOS). *Atmos. Chem. Phys. Discuss.* **2020**, *4*, 1–30. [CrossRef]
47. Zhang, Z.; Zimmermann, N.E.; Stenke, A.; Li, X.; Hodson, E.L.; Zhu, G.; Huang, C.; Poulter, B. Emerging role of wetland methane emissions in driving 21st century climate change. *Proc. Natl. Acad. Sci. USA* **2017**, *114*, 9647–9652. [CrossRef]
48. Zhang, Z.; Zimmermann, N.E.; Calle, L.; Hurtt, G.; Chatterjee, A.; Poulter, B. Enhanced response of global wetland methane emissions to the 2015–2016 El Niño-Southern Oscillation event. *Environ. Res. Lett.* **2018**, *13*, 074009. [CrossRef]
49. O'Neill, P.E.; Chan, E.G.S.; Jackson, N.T.; Bindlish, R.; Chaubell, J. *SMAP L3 Radiometer Global Daily 36 km EASE-Grid Soil Moisture, Version 6*; National Snow and Ice Data Center: Boulder, CO, USA, 2019. [CrossRef]
50. Das, N.N.; Entekhabi, D.; Njoku, E.G. An Algorithm for Merging SMAP Radiometer and Radar Data for High-Resolution Soil-Moisture Retrieval. *IEEE Trans. Geosci. Remote Sens.* **2011**, *49*, 1504–1512. [CrossRef]
51. Entekhabi, D.; Reichle, R.H.; Koster, R.D.; Crow, W.T. Performance Metrics for Soil Moisture Retrievals and Application Requirements. *J. Hydrometeorol.* **2010**, *11*, 832–840. [CrossRef]
52. Zheng, D.; Li, X.; Wang, X.; Wang, Z.; Wen, J.; van der Velde, R.; Schwank, M.; Su, Z. Sampling depth of L-band radiometer measurements of soil moisture and freeze-thaw dynamics on the Tibetan Plateau. *Remote Sens. Environ.* **2019**, *226*, 16–25. [CrossRef]
53. Escorihuela, M.J.; Chanzy, A.; Wigneron, J.P.; Kerr, Y.H. Effective soil moisture sampling depth of L-band radiometry: A case study. *Remote Sens. Environ.* **2010**, *114*, 995–1001. [CrossRef]
54. Entekhabi, D.; Yueh, S.; de Lannoy, G. *SMAP Handbook*; Jet Propulsion Laboratory, California Institute of Technology: Pasadena ,CA, USA, 2014.
55. McColl, K.A.; Alemohammad, S.H.; Akbar, R.; Konings, A.G.; Yueh, S.; Entekhabi, D. The global distribution and dynamics of surface soil moisture. *Nat. Geosci.* **2017**, *10*, 100–104. [CrossRef]
56. Gianotti, D.J.S.; Salvucci, G.D.; Akbar, R.; McColl, K.A.; Cuenca, R.; Entekhabi, D. Landscape Water Storage and Subsurface Correlation From Satellite Surface Soil Moisture and Precipitation Observations. *Water Resour. Res.* **2019**, *55*, 9111–9132. [CrossRef]
57. Akbar, R.; Gianotti, D.S.; McColl, K.A.; Haghighi, E.; Salvucci, G.D.; Entekhabi, D. Hydrological Storage Length Scales Represented by Remote Sensing Estimates of Soil Moisture and Precipitation. *Water Resour. Res.* **2018**, *54*, 1476–1492. [CrossRef]
58. Gruber, A.; de Lannoy, G.; Albergel, C.; Al-Yaari, A.; Brocca, L.; Calvet, J.-C.; Colliander, A.; Cosh, M.; Crow, W.; Dorigo, W.; et al. Validation practices for satellite soil moisture retrievals: What are (the) errors? *Remote Sens. Environ.* **2020**, *244*, 111806. [CrossRef]
59. Reichle, R.H.; Koster, R.D.; Dong, J.; Berg, A.A. Global Soil Moisture from Satellite Observations, Land Surface Models, and Ground Data: Implications for Data Assimilation. *J. Hydrometeorol.* **2004**, *5*, 430–442. [CrossRef]
60. Raoult, N.; Delorme, B.; Ottlé, C.; Peylin, P.; Bastrikov, V.; Maugis, P.; Polcher, J. Confronting Soil Moisture Dynamics from the ORCHIDEE Land Surface Model with the ESA-CCI Product: Perspectives for Data Assimilation. *Remote Sens.* **2018**, *10*, 1786. [CrossRef]
61. Qiu, J.; Crow, W.T.; Nearing, G.S. The Impact of Vertical Measurement Depth on the Information Content of Soil Moisture for Latent Heat Flux Estimation. *J. Hydrometeorol.* **2016**, *17*, 2419–2430. [CrossRef]
62. Harris, I.; Osborn, T.J.; Jones, P.; Lister, D. Version 4 of the CRU TS monthly high-resolution gridded multivariate climate dataset. *Sci. Data* **2020**, *7*, 109. [CrossRef]
63. Crow, W.T.; Berg, A.A.; Cosh, M.H.; Loew, A.; Mohanty, B.P.; Panciera, R.; de Rosnay, P.; Ryu, D.; Walker, J.P. Upscaling sparse ground-based soil moisture observations for the validation of coarse-resolution satellite soil moisture products. *Rev. Geophys.* **2012**, *50*, RG2002. [CrossRef]
64. Knox, S.H.; Jackson, R.B.; Poulter, B.; McNicol, G.; Fluet-Chouinard, E.; Zhang, Z.; Hugelius, G.; Bousquet, P.; Canadell, J.G.; Saunois, M.; et al. FLUXNET-CH_4 Synthesis Activity: Objectives, Observations, and Future Directions. *Bull. Am. Meteor. Soc.* **2019**, *100*, 2607–2632. [CrossRef]
65. Gruber, N.; Clement, D.; Carter, B.R.; Feely, R.A.; van Heuven, S.; Hoppema, M.; Ishii, M.; Key, R.M.; Kozyr, A.; Lauvset, S.K.; et al. The oceanic sink for anthropogenic CO_2 from 1994 to 2007. *Science* **2019**, *363*, 1193–1199. [CrossRef] [PubMed]
66. Jung, M.; Reichstein, M.; Bondeau, A. Towards global empirical upscaling of FLUXNET eddy covariance observations: Validation of a model tree ensemble approach using a biosphere model. *Biogeosciences* **2009**, *13*, 2001–2013. [CrossRef]

67. Jung, M.; Koirala, S.; Weber, U.; Ichii, K.; Gans, F.; Camps-Valls, G.; Papale, D.; Schwalm, C.; Tramontana, G.; Reichstein, M. The FLUXCOM ensemble of global land-atmosphere energy fluxes. *Sci. Data* **2019**, *6*, 74. [CrossRef] [PubMed]
68. Taylor, K.E. Summarizing multiple aspects of model performance in a single diagram. *J. Geophys. Res. Atmos.* **2001**, *106*, 7183–7192. [CrossRef]
69. Dietze, M.C.; Vargas, R.; Richardson, A.D.; Stoy, P.C.; Barr, A.G.; Anderson, R.S.; Arain, M.A.; Baker, I.T.; Black, T.A.; Chen, J.M.; et al. Characterizing the performance of ecosystem models across time scales: A spectral analysis of the North American Carbon Program site-level synthesis. *J. Geophys. Res. Biogeosci.* **2011**, *116*, G04029. [CrossRef]
70. Stoy, P.C.; Dietze, M.C.; Richardson, A.D.; Vargas, R.; Barr, A.G.; Anderson, R.S.; Arain, M.A.; Baker, I.T.; Black, T.A.; Chen, J.M.; et al. Evaluating the agreement between measurements and models of net ecosystem exchange at different times and timescales using wavelet coherence: An example using data from the North American Carbon Program Site-Level Interim Synthesis. *Biogeosciences* **2013**, *10*, 6893–6909. [CrossRef]
71. Vargas, R.; Detto, M.; Baldocchi, D.D.; Allen, M.F. Multiscale analysis of temporal variability of soil CO_2 production as influenced by weather and vegetation. *Glob. Chang. Biol.* **2010**, *16*, 1589–1605. [CrossRef]
72. Al-Yaari, A.; Wigneron, J.-P.; Ducharne, A.; Kerr, Y.; de Rosnay, P.; de Jeu, R.; Govind, A.; Al Bitar, A.; Albergel, C.; Muñoz-Sabater, J.; et al. Global-scale evaluation of two satellite-based passive microwave soil moisture datasets (SMOS and AMSR-E) with respect to Land Data Assimilation System estimates. *Remote Sens. Environ.* **2014**, *149*, 181–195. [CrossRef]
73. Jin, M.; Zheng, X.; Jiang, T.; Li, X.; Li, X.-J.; Zhao, K. Evaluation and Improvement of SMOS and SMAP Soil Moisture Products for Soils with High Organic Matter over a Forested Area in Northeast China. *Remote Sens.* **2017**, *9*, 387. [CrossRef]
74. Zhang, R.; Kim, S.; Sharma, A. A comprehensive validation of the SMAP Enhanced Level-3 Soil Moisture product using ground measurements over varied climates and landscapes. *Remote Sens. Environ.* **2019**, *223*, 82–94. [CrossRef]
75. O'Neill, P.; Chan, S.; Colliander, A.; Dunbar, S.; Njoku, E.; Bindlish, R.; Chen, F.; Jackson, T.; Burgin, M.; Piepmeier, J.; et al. Evaluation of the validated Soil Moisture product from the SMAP radiometer. In Proceedings of the 2016 IEEE International Geoscience and Remote Sensing Symposium (IGARSS), Beijing, China, 10–15 July 2016; pp. 125–128.
76. Al-Yaari, A.; Wigneron, J.-P.; Kerr, Y.; Rodriguez-Fernandez, N.; O'Neill, P.E.; Jackson, T.J.; de Lannoy, G.J.M.; Al Bitar, A.; Mialon, A.; Richaume, P.; et al. Evaluating soil moisture retrievals from ESA's SMOS and NASA's SMAP brightness temperature datasets. *Remote Sens. Environ.* **2017**, *193*, 257–273. [CrossRef]
77. Bastos, A.; Ciais, P.; Friedlingstein, P.; Sitch, S.; Pongratz, J.; Fan, L.; Wigneron, J.P.; Weber, U.; Reichstein, M.; Fu, Z.; et al. Direct and seasonal legacy effects of the 2018 heat wave and drought on European ecosystem productivity. *Sci. Adv.* **2020**, *6*, eaba2724. [CrossRef] [PubMed]
78. De Kauwe, M.G.; Zhou, S.-X.; Medlyn, B.E.; Pitman, A.J.; Wang, Y.-P.; Duursma, R.A.; Prentice, I.C. Do land surface models need to include differential plant species responses to drought? Examining model predictions across a mesic-xeric gradient in Europe. *Biogeosciences* **2015**, *12*, 7503–7518. [CrossRef]
79. Le Vine, N.; Butler, A.; McIntyre, N.; Jackson, C. Diagnosing hydrological limitations of a land surface model: Application of JULES to a deep-groundwater chalk basin. *Hydrol. Earth Syst. Sci.* **2016**, *20*, 143–159. [CrossRef]
80. Ukkola, A.M.; Pitman, A.J.; Decker, M.; de Kauwe, M.G.; Abramowitz, G.; Kala, J.; Wang, Y.-P. Modelling evapotranspiration during precipitation deficits: Identifying critical processes in a land surface model. *Hydrol. Earth Syst. Sci.* **2016**, *20*, 2403–2419. [CrossRef]
81. Lunt, M.F.; Palmer, P.I.; Feng, L.; Taylor, C.M.; Boesch, H.; Parker, R.J. An increase in methane emissions from tropical Africa between 2010 and 2016 inferred from satellite data. *Atmos. Chem. Phys.* **2019**, *19*, 14721–14740. [CrossRef]
82. Lunt, M.F.; Palmer, P.I.; Lorente, A.; Borsdorff, T.; Landgraf, J.; Parker, R.J.; Boesch, H. Rain-fed pulses of methane from East Africa during 2018–2019 contributed to atmospheric growth rate. *Environ. Res. Lett.* **2021**, *16*, 024021. [CrossRef]
83. Pandey, S.; Houweling, S.; Lorente, A.; Borsdorff, T.; Tsivlidou, M.; Bloom, A.A.; Poulter, B.; Zhang, Z.; Aben, I. Using satellite data to identify the methane emission controls of South Sudan's wetlands. *Biogeosciences* **2021**, *18*, 557–572. [CrossRef]
84. Koster, R.D.; Milly, P.C.D. The Interplay between Transpiration and Runoff Formulations in Land Surface Schemes Used with Atmospheric Models. *J. Clim.* **1997**, *10*, 1578–1591. [CrossRef]
85. Saleem, J.A.; Salvucci, G.D. Comparison of Soil Wetness Indices for Inducing Functional Similarity of Hydrologic Response across Sites in Illinois. *J. Hydrometeorol.* **2002**, *3*, 80–91. [CrossRef]
86. Albergel, C.; Rüdiger, C.; Pellarin, T.; Calvet, J.-C.; Fritz, N.; Froissard, F.; Suquia, D.; Petitpa, A.; Piguet, B.; Martin, E. From near-surface to root-zone soil moisture using an exponential filter: An assessment of the method based on in-situ observations and model simulations. *Hydrol. Earth Syst. Sci.* **2008**, *12*, 1323–1337. [CrossRef]
87. Alvarez-Garreton, C.; Ryu, D.; Western, A.W.; Crow, W.T.; Su, C.-H.; Robertson, D.R. Dual assimilation of satellite soil moisture to improve streamflow prediction in data-scarce catchments. *Water Resour. Res.* **2016**, *52*, 5357–5375. [CrossRef]
88. Wagner, W.; Lemoine, G.; Rott, H. A Method for Estimating Soil Moisture from ERS Scatterometer and Soil Data. *Remote Sens. Environ.* **1999**, *70*, 191–207. [CrossRef]
89. Colliander, A.; Jackson, T.J.; Bindlish, R.; Chan, S.; Das, N.; Kim, S.B.; Cosh, M.H.; Dunbar, R.S.; Dang, L.; Pashaian, L.; et al. Validation of SMAP surface soil moisture products with core validation sites. *Remote Sens. Environ.* **2017**, *191*, 215–231. [CrossRef]
90. Park, C.-H.; Montzka, C.; Jagdhuber, T.; Jonard, F.; Lannoy, G.D.; Hong, J.; Jackson, T.J.; Wulfmeyer, V. A Dielectric Mixing Model Accounting for Soil Organic Matter. *Vadose Zone J.* **2019**, *18*, 190036. [CrossRef]

91. Polcher, J.; Piles, M.; Gelati, E.; Barella-Ortiz, A.; Tello, M. Comparing surface-soil moisture from the SMOS mission and the ORCHIDEE land-surface model over the Iberian Peninsula. *Remote Sens. Environ.* **2016**, *174*, 69–81. [CrossRef]
92. Reichle, R.H.; McLaughlin, D.B.; Entekhabi, D. Hydrologic Data Assimilation with the Ensemble Kalman Filter. *Mon. Weather Rev.* **2002**, *130*, 103–114. [CrossRef]
93. Peylin, P.; Bacour, C.; MacBean, N.; Leonard, S.; Rayner, P.; Kuppel, S.; Koffi, E.; Kane, A.; Maignan, F.; Chevallier, F.; et al. A new stepwise carbon cycle data assimilation system using multiple data streams to constrain the simulated land surface carbon cycle. *Geosci. Model Dev.* **2016**, *9*, 3321–3346. [CrossRef]